*Nucleic Acids Research*, 2024, **52**, 1156–1172
https://doi.org/10.1093/nar/gkad1176
Advance access publication date: 6 December 2023
**Genome integrity, repair and replication**

# Spatial regulation of DNA damage tolerance protein Rad5 interconnects genome stability maintenance and proteostasis networks

**Carl P. Lehmann, Paula González-Fernández and José Antonio Tercero** *

Centro de Biología Molecular Severo Ochoa (CSIC/UAM), Cantoblanco. 28049-Madrid, Spain

*To whom correspondence should be addressed. Tel: +34 911964818; Fax: +34 911964420; Email: jatercero@cbm.csic.es

## Abstract

The Rad5/HLTF protein has a central role in the tolerance to DNA damage by mediating an error-free mode of bypassing unrepaired DNA lesions, and is therefore critical for the maintenance of genome stability. We show in this work that, following cellular stress, Rad5 is regulated by relocalization into two types of nuclear foci that coexist within the same cell, which we termed 'S' and 'I'. Rad5 S-foci form in response to genotoxic stress and are associated with Rad5's function in maintaining genome stability, whereas I-foci form in the presence of proteotoxic stress and are related to Rad5's own proteostasis. Rad5 accumulates into S-foci at DNA damage tolerance sites by liquid-liquid phase separation, while I-foci constitute sites of chaperone-mediated sequestration of Rad5 at the intranuclear quality control compartment (INQ). Relocalization of Rad5 into each type of foci involves different pathways and recruitment mechanisms, but in both cases is driven by the evolutionarily conserved E2 ubiquitin-conjugating enzyme Rad6. This coordinated differential relocalization of Rad5 interconnects DNA damage response and proteostasis networks, highlighting the importance of studying these homeostasis mechanisms in tandem. Spatial regulation of Rad5 under cellular stress conditions thus provides a useful biological model to study cellular homeostasis as a whole.

## Graphical abstract

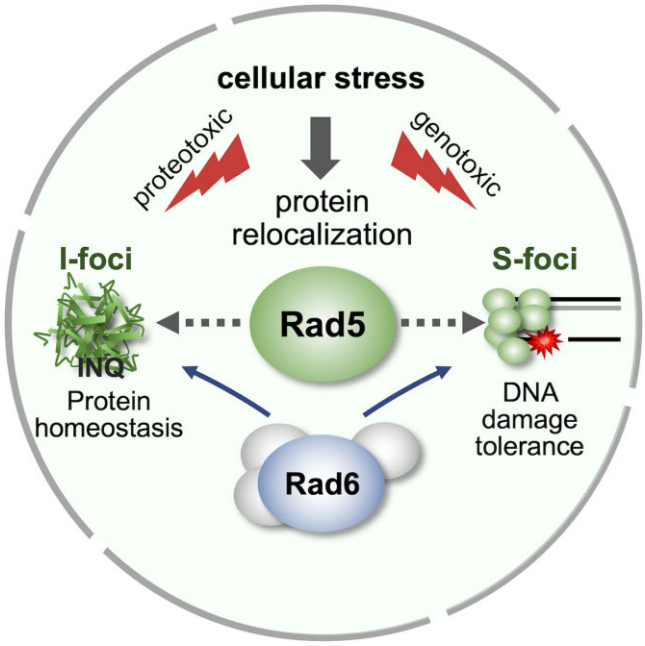


## Introduction

Cellular stress arises from multiple endogenous and exogenous sources and is a main cause of damage to both DNA and proteins. DNA damage originated by genotoxic stress is especially detrimental during chromosomal replication, as unrepaired non-bypassed lesions can cause permanent fork stalling or collapse that would result in incomplete genome replication, leading to genomic instability (1,2). Protein damage brought about by proteotoxic stress can result in non-functional, usually misfolded proteins, leading to protein

**Received:** August 22, 2023. **Revised:** November 21, 2023. **Editorial Decision:** November 21, 2023. **Accepted:** November 23, 2023

homeostasis loss (3). While generally studied independently, genomic instability and proteostasis loss are frequently intertwined. This is exemplified by situations of cellular stress that damage not only DNA but also proteins involved in coping with DNA lesions, leading to less efficient or compromised responses to maintain genome integrity. Moreover, genome and proteome instability often aggravate one another in a vicious cycle that can lead to cellular pathologies and disease, as occurs for example in some cancers and neurodegenerative diseases (4,5). DNA damage response and proteostasis networks help cells cope with genotoxic and proteotoxic stress, respectively (6,7), and both share protein relocalization as a hallmark (8–11). The study of this common hallmark is therefore important to investigate the possible interconnections between these networks.

In this work, we have studied the relocalization in response to cellular stress of budding yeast Rad5 (human HLTF), a key protein for the maintenance of genome stability. We found that its spatial regulation is a good model to address how DNA damage and proteotoxic stress responses are interconnected by protein relocalization. Rad5 is an E3-ubiquitin ligase and ATPase/helicase that belongs to the evolutionarily conserved *RAD6/RAD18* pathway of DNA damage tolerance (DDT). This pathway allows for bypassing fork-blocking DNA lesions, facilitating the completion of chromosome replication and thus cell survival (12–15). Following replication fork stalling caused by unrepaired DNA lesions or replicative stress, the DNA polymerases and the replicative helicase can uncouple, originating long ssDNA fragments. These are covered by RPA, which acts as a signal for the recruitment of the E3 ubiquitin ligase Rad18 to chromatin, which recruits the E2 ubiquitin-conjugating enzyme Rad6 (16). Rad18 and Rad6 form a heterodimer that monoubiquitylates PCNA at its K164 residue (17). This PCNA modification triggers translesion DNA synthesis (TLS) by facilitating the substitution of the replicative polymerases for TLS polymerases (18), which are specialized low-fidelity DNA polymerases that are able to replicate through DNA lesions in an error-prone and often mutagenic process (19). Monoubiquitylation of PCNA can be further extended to K63-linked polyubiquitin chains, which is carried out by Rad5 together with the E2 complex Ubc13-Mms2 (UBC13-UEV1 in mammals). PCNA polyubiquitylation promotes a second mode of DNA lesion bypass that is driven by the DNA-dependent ATPase/helicase activity of Rad5 and is carried out by transient template switch recombination (12–14,20). This mechanism uses the newly synthesized strand of the sister chromatid as a template to replicate over the lesion in a usually error-free process. Notably, in addition to its important role in mediating template switching for DNA damage bypass, Rad5 is also involved in modulating translesion DNA synthesis (21–23), thus making it a central protein in DDT.

Rad5 relocalizes and forms nuclear foci following treatment with model DNA-damaging agents such as the alkylating drug methyl methanesulfonate (MMS) (8,24,25), and also in response to DNA lesion-less replicative stress (8,21). While the latter have been well characterized and associated with stressed replication forks (21), little is known about the nature or relevance of Rad5 foci induced by DNA-damaging or other cellular stress-inducing agents. We show here that, after treatment of cells with various sources of cellular stress, Rad5 is differentially recruited into two types of nuclear foci that coexist within the same cell. One type of foci is related to Rad5's function in coping with DNA damage, while the other is associated with Rad5's own homeostasis. We show that the formation of each type of foci occurs via different pathways and requires distinct recruitment mechanisms, but both are linked to each other through a common dependency on Rad6, which is revealed as a key factor that interconnects genome and proteome stability networks.

## Materials and Methods

### Reagents and resources

Reagents and resources used in this work are listed in Table 1, together with their source and catalogue reference when appropriate.

### Yeast strains and media

*Saccharomyces cerevisiae* strains used in this work are listed with their relevant genotypes in Supplementary Table S1. They are all derived from W303 and corrected for *RAD5*. All strains were constructed by transformation with PCR-products or by crosses and subsequent tetrad dissection, using standard techniques. All fluorescent strains were tagged at their native loci. All strains were verified by PCR and drug sensitivity assays, as well as by immunoblot and DNA sequencing when appropriate. For epitope-tagging and gene deletions, the pML (26), pYM (29) and pRS (28) plasmid series were used as templates for PCR together with oligonucleotides listed in Supplementary Table S2. Yeasts were routinely grown in YP medium (1% Bacto-yeast extract, 2% Bacto-peptone, Becton Dickinson) supplemented with 2% glucose (Merck) at 30°C. For fluorescence microscopy experiments, cells were grown at 30°C in synthetic complete media: 0.67% yeast nitrogen base without amino acids (Becton Dickinson), 0.1% synthetic complete drop-out mixture (Kaiser), 2% glucose (Merck), and 0.013% adenine sulphate dihydrate (Sigma-Aldrich).

### Cell cycle synchronization and flow cytometry

Cells were synchronized in G1 using α-factor (5–10 μg/ml, Quimigen) and in G2/M with nocodazole (2 μg/ml, Sigma-Aldrich). To analyse cells in S phase, G1-blocked cells were washed twice with culture media and released into fresh media. In all cases, cell cycle synchronization was monitored by microscopic observation. Cell cycle stage was monitored by analysing the DNA content of cells by flow cytometry. Flow cytometry was basically as described (30): A 0.5–1 ml sample of culture was collected, centrifuged, fixed in 70% ethanol, and stored at 4°C. 50–200 μl of fixed cells were rehydrated in 3 ml of 50 mM sodium citrate and centrifuged at 1400 × g for 3 min. They were then resuspended in 0.5 ml of 50 mM sodium citrate with 0.1 mg/ml RNase A (Sigma-Aldrich) and incubated at 37°C for 2–4 h. Afterwards, cells were centrifuged again at 1400 × g for 3 min, resuspended in 0.5 ml of 50 mM HCl with 5 mg/ml pepsin (Sigma-Aldrich), and incubated at 37°C for 30 min. Cells were centrifuged once more at 1400 × g for 3 min and resuspended in 1 ml of 50 mM sodium citrate with 2 μg/ml propidium iodide (Sigma-Aldrich). Before running samples through the cytometer, they were briefly sonicated to disrupt any cellular aggregates. The DNA content of the cells was analysed using a FACScalibur cytometer (BD Biosciences) together with the software CellQuestPro (BD Biosciences).

**Table 1.** Main reagents and resources used in this work

| Reagent or resource | Source | Identifier |
|---|---|---|
| **Antibodies** | | |
| Mouse anti-GFP | Roche | Cat# 11814460001 |
| Rabbit anti-mCherry | J. M. Requena, CBMSO | N/A |
| HRP-anti-mouse | Vector Labs | Cat# PI-2000 |
| HRP-Protein A | Invitrogen | Cat# 10–1023 |
| **Chemicals, peptides** | | |
| 1,6-Hexanediol | Sigma-Aldrich | Cat# 240117 |
| 4-Nitroquinoline 1-oxide (4NQO) | Sigma-Aldrich | Cat# N8141 |
| α factor | Quimigen | N/A |
| L-Azetidine-2-carboxylic acid (AZC) | Sigma-Aldrich | Cat# A0760 |
| Cisplatin | Sigma-Aldrich | Cat# 232120 |
| Digitonin | Sigma-Aldrich | Cat# D141 |
| DMSO | Sigma-Aldrich | Cat# D2650 |
| Hydrogen peroxide | Peroxfarma | N/A |
| Hydroxyurea (HU) | Molekula | Cat# 10872383 |
| Methyl methanesulfonate (MMS) | Sigma-Aldrich or Thermo Fisher | Cat# 129925 Cat# H55120.06 |
| MG132 | MedChemExpress | Cat# HY-13259 |
| Nocodazole | Sigma-Aldrich | Cat# M1404 |
| Zeocin | Invitrogen | Cat# 11508976 |
| **Organisms/strains** | | |
| *Saccharomyces cerevisiae* strains, background: W303 See Supplementary Table S1 | This Manuscript | N/A |
| **Oligonucleotides** | | |
| Oligonucleotides used for strain construction, testing, and sequencing. See Supplementary Table S2 | This Manuscript. Purchased from IDT | N/A |
| **Plasmid vectors** | | |
| Plasmid: pFA6a-*URA3* | Helle Ulrich (IMB, Germany) | N/A |
| Plasmid: pFA6a-*kanMX6* | Longtine *et al.* (26) | N/A |
| Plasmid: pFA6a-*mCherry-hphNT1* | Saugar *et al.* (27) | N/A |
| Plasmid: pFA6a-*TRP1* | Longtine *et al.* (26) | N/A |
| Plasmid: pRS304 (*TRP1)* | Sikorski and Hieter (28) | N/A |
| Plasmid: pRS305 (*LEU2)* | Sikorski and Hieter (28) | N/A |
| Plasmid: pRS306 (*URA3)* | Sikorski and Hieter (28) | N/A |
| Plasmid: pYM44 (pFA6a-*yeGFP-HisMX6*) | Janke *et al.* (29) | N/A |
| **Software and algorithms** | | |
| FIJI | ImageJ2 | https://imagej.net/software/fiji/ |
| Huygens Deconvolution | SVI | https://svi.nl/Huygens-Professional |
| Adobe Photoshop | Adobe | https://www.adobe.com |
| GraphPad PRISM v8.2.1 | GraphPad Software | https://www.graphpad.com |
| CellQuestPro v6.1 | BD Biosciences | https://www.bdbiosciences.com |

## Drug treatments to analyse foci formation

MMS treatments were as indicated in the text in each case. For the other drugs used, cycling cells were treated for 60 min, except AZC (120 min), as follows: 200 mM hydroxyurea (HU), 0.5 mM cisplatin, 0.5 μg/ml 4NQO, 100 μg/ml zeocin, 0.4 mM $H_2O_2$, 1 mg/ml L-azetidine-2-carboxilic acid (AZC). DMSO (solvent) was used as a control for cisplatin.

## Drug sensitivity assay

Cell viability after MMS treatment during a single S phase was determined by plating approximately 500 cells in triplicate onto YP-glucose plates and counting colony forming units after 72 h of incubation at 30ºC.

## Immunoblot analysis

Protein extracts for immunoblot analysis were prepared from approximately $10^8$ TCA-treated cells as described (31). Proteins were transferred to nitrocellulose membranes (Amersham Protran Premium Blotting membranes, GE Healthcare) using semi-dry transfer. GFP- and mCherry-tagged proteins were detected with anti-GFP and anti-mCherry antibodies (Table 1), using HRP-anti-mouse and HRP-Protein A (Table 1) as secondary antibodies. Immunoreactive bands were visualized using enhanced chemiluminescence (ECL prime, GE Healthcare).

## Live-cell fluorescence microscopy

Cells were grown to exponential phase in synthetic complete media at 30ºC, synchronized when required at the appropriate stage of the cell cycle, and treated with the indicated cellular stress agent. After treatment, 20–25 ml of culture were centrifuged at 2031 × g for 2 min, and the pellet was resuspended in 0.5 ml of reserved supernatant and then transferred to a 1.5 ml tube and briefly sonicated. A 5 μl sample of cells was placed on a Polysine® (Epredia) slide and covered with a 22 × 22 mm coverslip. The edges of the slide were sealed with Twinsil (Picodent) and the sample was taken immediately to the microscope for analysis. Cells were visualized using an IX83 inverted confocal microscope with a SpinSR10 spinning disk module (Olympus), a 100× oil immersion extended apochromat objective with 1.45 NA, a CSU-W1 scanner with a SoRa disk (Yokogawa), 488 nm and 561 nm DPSS lasers, GFP and TRITC filters, a sCMOS Prime 95B

camera (Photometrics), and CellSens imaging software. For each field of cells captured, a stack of 20–25 fluorescent images was obtained along the z axis at 0.2 μm intervals, along with a single Nomarski image. The fluorescent image stacks were deconvoluted using Huygens Deconvolution (SVI) software, converted into Z projections using Fiji, and then quantified manually. Prepared images were cropped using Adobe Photoshop. The percentage of cells containing foci and/or colocalization was calculated as an average of three independent experiments. At least 200 cells were counted in each experiment.

### Time-lapse microscopy

G1-synchronized cells were released into S phase in the presence of 0.033% MMS for 60 min and then taken to the microscope to start the time-lapse. Once per minute, for 3 min, a stack of 20 florescent images was obtained along the z axis at 0.2 μm intervals.

### Statistical analyses

All experiments were performed with at least three biological repeats, except the one in Figure 6E, F, which was conducted in duplicate. Numerical data are represented as mean ± standard deviation (s.d.). Statistical analysis was performed using an unpaired two-tailed Student's *t*-test. A $P$ value of $< 0.01$ was considered statistically significant. For simplicity in the figures, only statistically significant $P$ values are shown.

## Results

### Rad5 is differentially recruited into two types of coexisting nuclear foci

Given its wide use as a model DNA damaging agent, we utilized MMS to begin our study of Rad5 relocalization. To investigate MMS-induced Rad5 foci, we used live-cell microscopy and *RAD5-yeGFP* expressed from its own promoter at its native locus. Treatment of exponentially growing *RAD5-yeGFP* cells with 0.033% MMS, conditions known to cause replication fork stalling (32), strongly induced Rad5 relocalization into discrete nuclear foci (Figure 1A), whereas the number of untreated cells with detectable Rad5 foci was very low, thus confirming previous data with different strain constructions and approaches (8,24,25). Rad5 accumulation into foci was not due to significant changes in protein levels after MMS treatment (Supplementary Figure S1A), thus reflecting protein relocalization. Cell-cycle analysis showed recruitment of Rad5 into foci following MMS treatment during G1 and S-phase, but not G2/M (Figure 1B and Supplementary Figure S1B). In G1 cells, Rad5 formed a single and usually perinuclear focus, whereas in S-phase cells Rad5 formed multiple foci (Supplementary Figure S1B). If these foci were related to protein function, as one might assume given that they form after DNA damage induced by MMS-treatment, it seems reasonable that they would appear during S-phase, when Rad5 carries out its DNA damage tolerance activities (12,24,33). However, as Rad5 foci also formed in G1, when Rad5 presumably has no role, they might represent sites of non-functioning accumulated protein.

As MMS-induced Rad5 foci were nuclear, we analysed whether they colocalized with any known nuclear structures marked by specific proteins. We did not observe significant colocalization of Rad5 foci with the spindle pole body (marked by SPC42), telomere clusters (Rap1), nucleolus (Nop1) or nuclear pore (Nup84) (Figure 1C and Supplementary Figure S1C, D). However, we found colocalization of Rad5 foci with the intranuclear quality control compartment (INQ, marked by Cmr1) in a high number of cells (Figure 1C and Supplementary Figure S1C, D). The INQ plays a role in protein homeostasis by accumulating proteins, frequently misfolded, in response to various types of stress (10,34–36), suggesting that protein quality control (PQC) may be a reason for Rad5 recruitment into foci. Additional analysis showed that, during G1, the single observed Rad5 focus colocalized with Cmr1, whereas in a high number of S-phase cells only one of the multiple foci colocalized with Cmr1 (Figure 1D–G and Supplementary Figure S1E). We concluded that, after MMS treatment, Rad5 is recruited into two types of foci: we termed 'I-foci' those that colocalize with Cmr1 at the INQ and form during G1 and S-phase, and 'S-foci' those that do not colocalize with Cmr1 and form exclusively during S-phase. Because a given cell may contain one or both types of foci, we defined four categories of cells (Figure 1G and Supplementary Figure S1E): (i) 'Only colocalization' describes cells with a single Rad5 focus that colocalizes with Cmr1 (Rad5 I-foci); (ii) 'No colocalization', cells with Rad5 foci that do not colocalize with Cmr1 (Rad5 S-foci); (iii) 'Mix colocalization', cells that contain a Rad5 focus that colocalizes with Cmr1 and Rad5 foci that do not (Rad5 I- and S-foci); (iv) 'Undefined', cells with Rad5 foci but no Cmr1 focus with which to compare their location. Besides their numerical and cell cycle differences, S-foci were dynamic and transient, while I-foci were more static and stable (Supplementary Movie S1).

### Rad6 drives the formation of both types of Rad5 foci via divergent pathways

To study the nature and importance of the two classes of Rad5 foci, we next investigated which might be the potential pathways involved in Rad5 relocalization. We found that formation of both types of foci is fully dependent on the evolutionarily conserved E2-ubiquitin conjugating enzyme Rad6 (Figure 2A and Supplementary Figure S2A). This protein is upstream of Rad5 in the DDT Rad6/Rad18 pathway (12,13,15,37) and is necessary for recruitment of endonucleases to the INQ after MMS treatment (27). Since Rad6 interacts with four E3-ubiquitin ligases (Rad18, Ubr1, Bre1, Ubr2) to carry out different functions via separate pathways (38–41), we analysed the potential relevance of all of them for the recruitment of Rad5 into foci.

Rad6 together with Rad18 monoubiquitylate PCNA at K164, triggering DDT mechanisms (17). In MMS-treated *rad18*Δ cells, Rad5 did not form S-foci, but it was recruited into I-foci (Figure 2A and Supplementary Figure S2A). This result was due to lack of PCNA monoubiquitylation, as *pol30K164R* mutant cells exhibited the same phenotype as *rad18*Δ cells for Rad5-foci formation, while cells lacking the E3-SUMO ligase Siz1, which is responsible for PCNA-sumoylation at K164 and K127 (17), displayed no defect (Figure 2A and Supplementary Figure S2A). Therefore, relocalization of Rad5 into S-foci requires a functional DNA damage tolerance pathway. Of note, DNA lesion-less replicative stress-induced Rad5 foci are also associated to a functional Rad6/Rad18 pathway and depend on PCNA monoubiquitylation (21), indicating that recruitment of Rad5

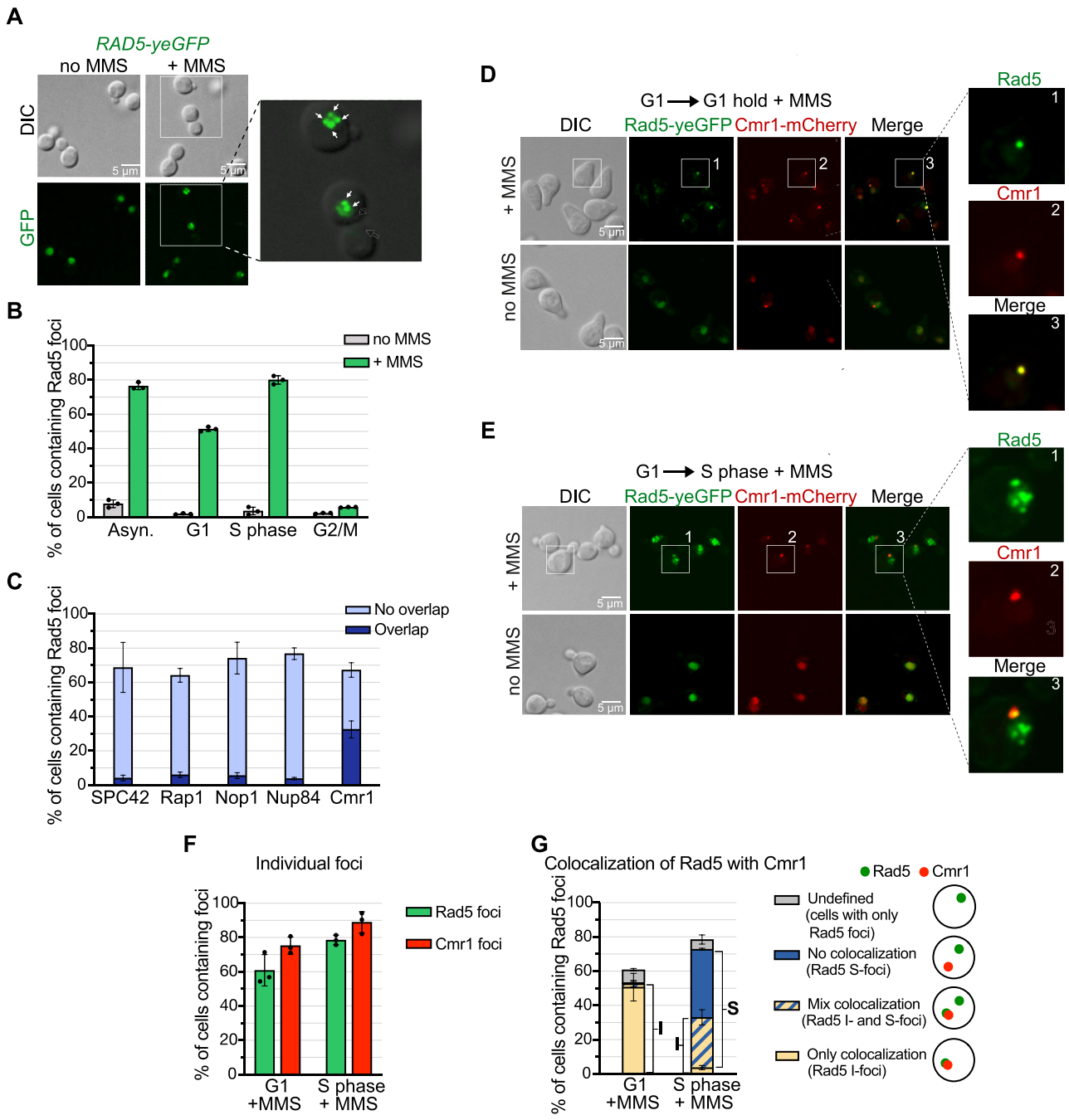


**Figure 1.** Rad5 is recruited into two types of nuclear foci in response to MMS treatment. (**A**) Fluorescence microscopy analysis of Rad5 foci formation. Cycling *RAD5-yeGFP* cells (YCL46 strain) were examined after treatment with 0.033% MMS for 60 min. Arrows indicate some foci examples. (**B**) Percentage of cells containing Rad5 foci in asynchronous cultures (data from A) and at different stages of the cell cycle. For G1 analysis, cells (YCL46 strain) were synchronized using $\alpha$ factor and held in G1 (–/+0.033% MMS, 60 min). For S phase analysis, G1-synchronized cells were released into S phase in fresh medium (+0.033% MMS, 60 min, or without MMS, 30 min). For G2/M analysis, cells were synchronized with nocodazole and held in G2/M (–/+0.033% MMS, 60 min). (**C**) Analysis of Rad5 foci subnuclear localization after MMS treatment (0.033% MMS, 60 min, logarithmic cultures). The figure shows quantification of the percentage of cells in which Rad5-yeGFP colocalizes with proteins that mark different nuclear structures: SPC42-eqFP (YCL171 strain), Rap1-mCherry (YCL173), Nop1-mCherry (YCL146), Nup84-mCherry (YCL169) or Cmr1-mCherry (YCL51). (**D**, **E**) Colocalization of Rad5-foci with Cmr1-foci (YCL51 strain). G1- (D) and S-phase (E) analyses were as described in (B). (**F**) Percentage of cells containing Rad5 or Cmr1 foci, from (D, E). (**G**) Percentage of cells containing Rad5 foci and their colocalization patterns with Cmr1 foci, from (D, E). Rad5 I- and S-foci are delineated in brackets. A diagram of the possible colocalization patterns between Rad5 and Cmr1 foci is shown. In all cases, the bar graphs represent the mean ± SD from three independent experiments. DIC: differential interference contrast (Nomarski): GFP: green fluorescent protein.

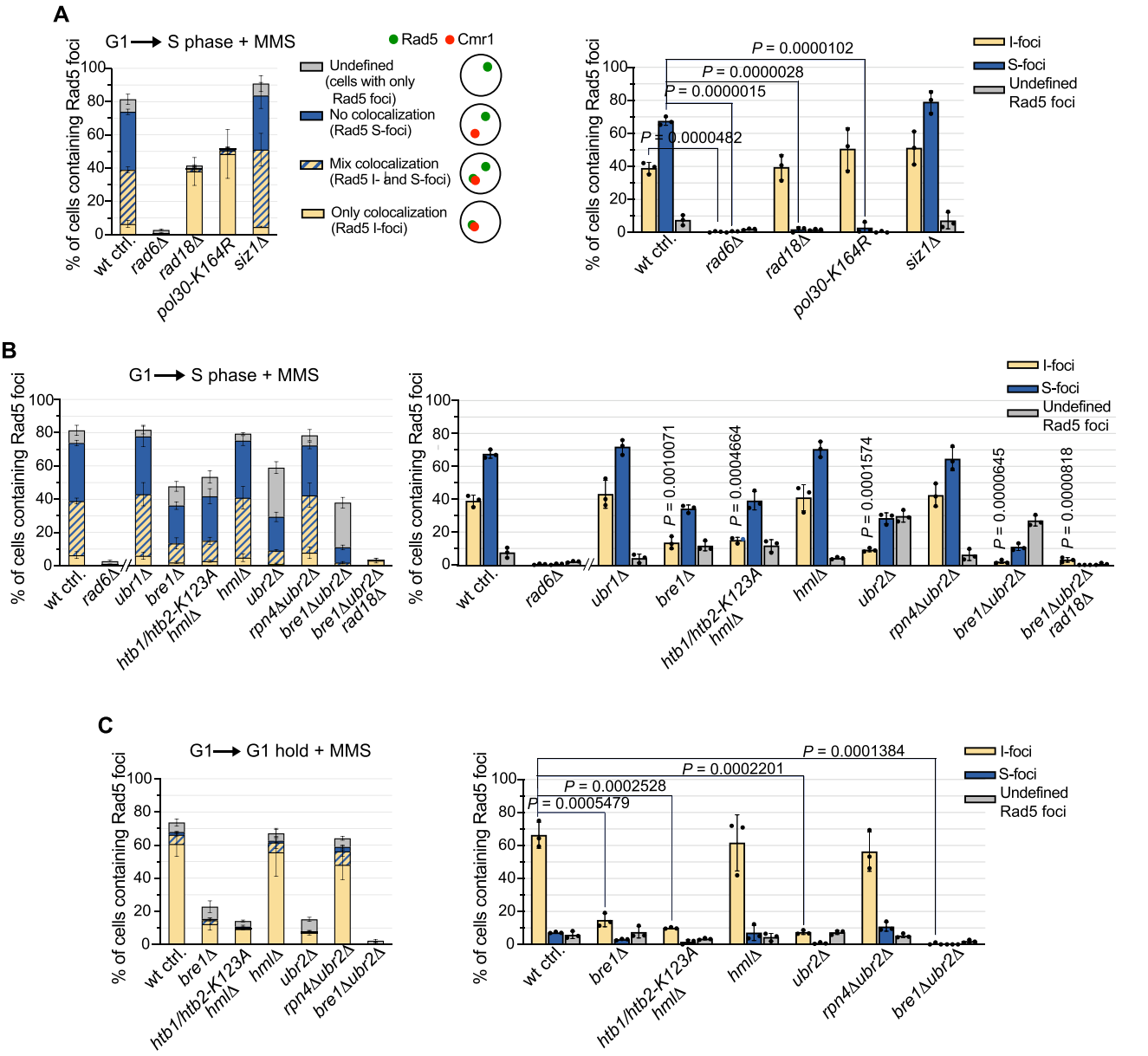


**Figure 2.** Rad6 is required for Rad5 S- and I-foci formation via distinct pathways. (**A**) Both Rad5 S- and I-foci depend on Rad6, and S-foci on Rad6/Rad18-mediated PCNA ubiquitylation. For S phase analysis, G1-synchronized cells were released into S phase in fresh medium (+0.033% MMS, 60 min) and analysed by fluorescence microscopy. Left panel shows data quantification. A diagram of the possible colocalization patterns between Rad5 and Cmr1 foci is shown. Right panel displays percentage of cells containing each type of Rad5 foci. The percentage of Rad5 I- or S-foci was calculated based on the total population of cells analysed using the data from left panel. Statistical significance was calculated between the percentage of cells with Rad5 I- or S-foci in the wild type-control and the corresponding Rad5 foci type of each mutant. Strains: wt-control (*RAD5-yeGFP CMR1-mCherry,* YCL51), *rad6*Δ (YCL149), *rad18*Δ (YCL126), *pol30-K164R* (YCL122), *siz1*Δ (YCL132). (**B**) Rad6/Bre1/histone H2B and Rad6/Ubr2/Rpn4 pathways contribute to Rad5 I-foci formation. For S phase analysis, G1-synchronized cells were released into S phase in fresh medium (+0.033% MMS, 60 min) and analysed by fluorescence microscopy. Left panel shows data quantification of the fluorescence microscopy analysis. Right panel displays percentage of cells containing each type of Rad5 foci, calculated based on the total population of cells analysed using the data from left panel. Statistical significance was calculated between the percentage of cells with Rad5 I-foci or S-foci in the wild type-control and each mutant. Strains: wt-control (YCL51), *rad6*Δ (YCL149), *ubr1*Δ (YCL151), *bre1*Δ (YCL133), *htb1/htb2-K123A hml*Δ (YCL231), *hml*Δ (YCL232), *ubr2*Δ (YCL154), *rpn4*Δ*ubr2*Δ (YCL237), *bre1*Δ*ubr2*Δ (YCL156), *rad18*Δ*bre1*Δ*ubr2*Δ (YCL177). wt-control and *rad6*Δ data are the same as in (A). The *htb1/htb2-K132A* mutant was combined with deletion of the HML locus to make cells responsive to $\alpha$ factor pheromone. (**C**) Rad6/Bre1/histone H2B and Rad6/Ubr2/Rpn4 pathways contribute to Rad5 I-foci formation. For G1 analysis, cells were synchronized using $\alpha$ factor and held in G1 (+0.033% MMS, 60 min). Left panel shows data quantification of the fluorescence microscopy analysis. Right panel displays percentage of cells containing each type of Rad5 foci, calculated based on the total population of cells analysed using the data from left panel. Statistical significance was calculated between the percentage of cells with Rad5 I-foci in the wild type-control and each mutant. Strains: wt-control (YCL51), *bre1*Δ (YCL133), *htb1/htb2-K123A hml*Δ (YCL231), *hml*Δ (YCL232), *ubr2*Δ (YCL154), *rpn4*Δ*ubr2*Δ (YCL237), *bre1*Δ*ubr2*Δ (YCL156). In all cases, the bar graphs represent the mean ± SD from three independent experiments. Only statistically significant *P* values ($P < 0.01$) are shown.

into both these foci and into MMS-induced S-foci requires the same relocalization signal.

In contrast to the requirement for Rad18, there was no effect on Rad5 foci formation in cells lacking the E3-ubiquitin ligase Ubr1 (Figure 2B and Supplementary Figure S2B), which is involved in protein degradation via the N-degron pathway (39). We then analysed cells lacking the E3-ubiquitin ligase Bre1, which mono-ubiquitylates histone H2B at K123, leading to chromatin remodelling and several downstream effects including transcriptional regulation (42). A *bre1*Δ mutant showed a strong decrease in the number of MMS-treated cells with Rad5 I-foci in S-phase, with minor effects on S-foci (Figure 2B and Supplementary Figure S2B). G1-analysis, which provides a cleaner result as G1-cells only contain I-foci (Figure 1D-G), also showed an important reduction in the number of *bre1*Δ cells with I-foci (Figure 2C and Supplementary Figure S2C). Moreover, a non-ubiquitylable histone H2B mutant (*htb1/htb2-K132A*) displayed a similar phenotype to *bre1*Δ (Figure 2B, C and Supplementary Figure S2B, C). Therefore, Rad5 recruitment into I-foci has a meaningful, albeit partial, Bre1-dependency via histone H2B ubiquitylation. We then examined the fourth known Rad6 E3-ubiquitin ligase partner, Ubr2. *ubr2*Δ cells also underwent a significant reduction in Rad5 I-foci in G1 and S-phase MMS-treated cells (Figure 2B, C and Supplementary Figure S2B, C). Ubr2 negatively regulates the transcription factor Rpn4 by ubiquitylation, favouring its degradation (40), which reduces the expression of proteasome genes. We reasoned that if the Rad5 I-foci dependency on Ubr2 were due to the described unchecked high levels of Rpn4 in *ubr2*Δ cells (43), *RPN4* deletion should rescue the depleted Rad5 I-foci in this background. As expected, MMS-treated *rpn4*Δ*ubr2*Δ cells showed a complete rescue of I-foci formation (Figures 2B, C, and Supplementary Figure S2B, C). Therefore, MMS-induced Rad5 I-foci have an important dependency on Rad6/Ubr2 ubiquitin-mediated downregulation of Rpn4, strongly suggesting that proteasome activity modulates their formation. Of note, Rad5 I-foci were absent in *bre1*Δ*ubr2*Δ cells (Figures 2B, C, and Supplementary Figure S2B, C), reflecting the requirement of both Rad6/Bre1/H2B and Rad6/Ubr2/Rpn4 pathways for I-foci formation. Furthermore, the triple mutant *rad18*Δ*bre1*Δ*ubr2*Δ showed neither I-foci nor S-foci (Figure 2B and Supplementary Figure S2B), phenocopying *rad6*Δ and confirming the full Rad6-dependency, via three of its pathways, for Rad5 relocalization.

## Rad5 is recruited into each type of foci through different mechanisms

Next, we studied the mechanisms by which Rad5 could be transported into each type of foci. We first analysed the potential involvement of the Btn2 chaperone in Rad5 relocalization, as it was shown necessary for the formation of the INQ compartment (10,27,34,35), where Rad5 I-foci are located. *btn2*Δ cells displayed no Rad5 I-foci after MMS treatment in G1 or S-phase, while S-foci were unaffected, indicating Btn2 is involved in sequestering Rad5 into I-foci (Figure 3A, B and Supplementary Figure S3A, B). Of note, *rad18*Δ*btn2*Δ cells showed no foci, phenocopying *rad6*Δ cells (Figure 3A, B and Supplementary Figure S3A), thus confirming that the 'undefined' Rad5-foci (those appearing in cells lacking Cmr1-foci) found in *btn2*Δ cells were indeed S-foci, since these depend on Rad18, as we showed in the previous section. Importantly, Btn2 itself forms stress-induced foci that localize to the INQ and cytoQ (34,44), the latter being a cytosolic PQC compartment. Moreover, Btn2 relocalization to INQ is necessary for the recruitment of other proteins to this compartment (44). As expected, MMS treatment induced relocalization of Btn2 into foci, some of which were nuclear, colocalizing with Rad5 at the INQ, while others were cytoplasmic, marking cytoQ (Figure 3C, D). Remarkably, in *rad6*Δ cells, Btn2 was barely recruited into foci (Figure 3D), indicating that Rad6 is a regulator of Btn2 relocalization. This result, together with the genetic dependencies shown above, present Rad6 as a master protein coordinating Rad5 foci formation via different pathways.

Given that Btn2 transports Rad5 specifically into I-foci but not S-foci, there should be another mechanism for Rad5 relocalization into the latter. A computer-generated model predicts Rad5 to contain several intrinsically disordered regions (IDRs) (Supplementary Figure S3C). IDRs participate in weak multivalent molecular interactions and are frequent in proteins that undergo liquid-liquid phase separation, resulting in the formation of liquid droplets (45,46). To analyse whether this could be the case for Rad5, we treated cells containing MMS-induced Rad5 foci with 1,6-hexanediol, which can dissolve liquid-like condensates *in vivo* (47–49). As a negative control we used the isomer 2,5-hexanediol, which has minimal condensate-dissolving activity (50,51). The treatment with 1,6-hexanediol, but not with 2,5-hexanediol, caused a sharp decrease in the number of cells containing S-foci, but not I-foci (Figure 3E, F and Supplementary Figure S3D, E), strongly indicating that the former may represent condensates formed by liquid-liquid phase separation.

## Genotoxic stress induces S-foci while proteotoxic stress gives rise to I-foci

The cellular stress agent we have used thus far, MMS, is generally regarded as genotoxic because it causes DNA damage (52). However, MMS can also methylate proteins, which may lead to protein misfolding (53–55) and could explain Rad5 recruitment into I-foci at the INQ compartment. If this were the case, we reasoned that I-foci formation should exhibit an MMS dose-dependent response. In agreement with this idea, treatment with a 'high' MMS concentration (0.33%) yielded a significant increase in the number of cells with I-foci in comparison with the 'standard' concentration used (0.033%) (Figure 4A and Supplementary Figure S4A). Interestingly, this treatment also caused a marked decrease in the number of cells containing S-foci (Figure 4A and Supplementary Figure S4A). These data suggest that the high MMS dose causes so much damage to Rad5 that most of the protein is recruited to the INQ with little functional protein left over for recruitment into S-foci. Conversely, treatment with a 'low' MMS concentration (0.0033%) induced only S-foci, as confirmed by the absence of undefined Rad5-foci when deleting *RAD18* (Figure 4A and Supplementary Figure S4A). This result correlates a low MMS dose, which still needs to be tolerated by Rad5 (24), with the presence of S-foci, and suggests only DNA is significantly damaged under these conditions, thereby relating these foci to DNA damage tolerance.

To further differentiate between DNA and protein insults and their relation with each type of foci, we treated cells with different cellular stress-inducing agents and analysed Rad5 foci formation (Figure 4B, C and Supplementary Figure S4B).

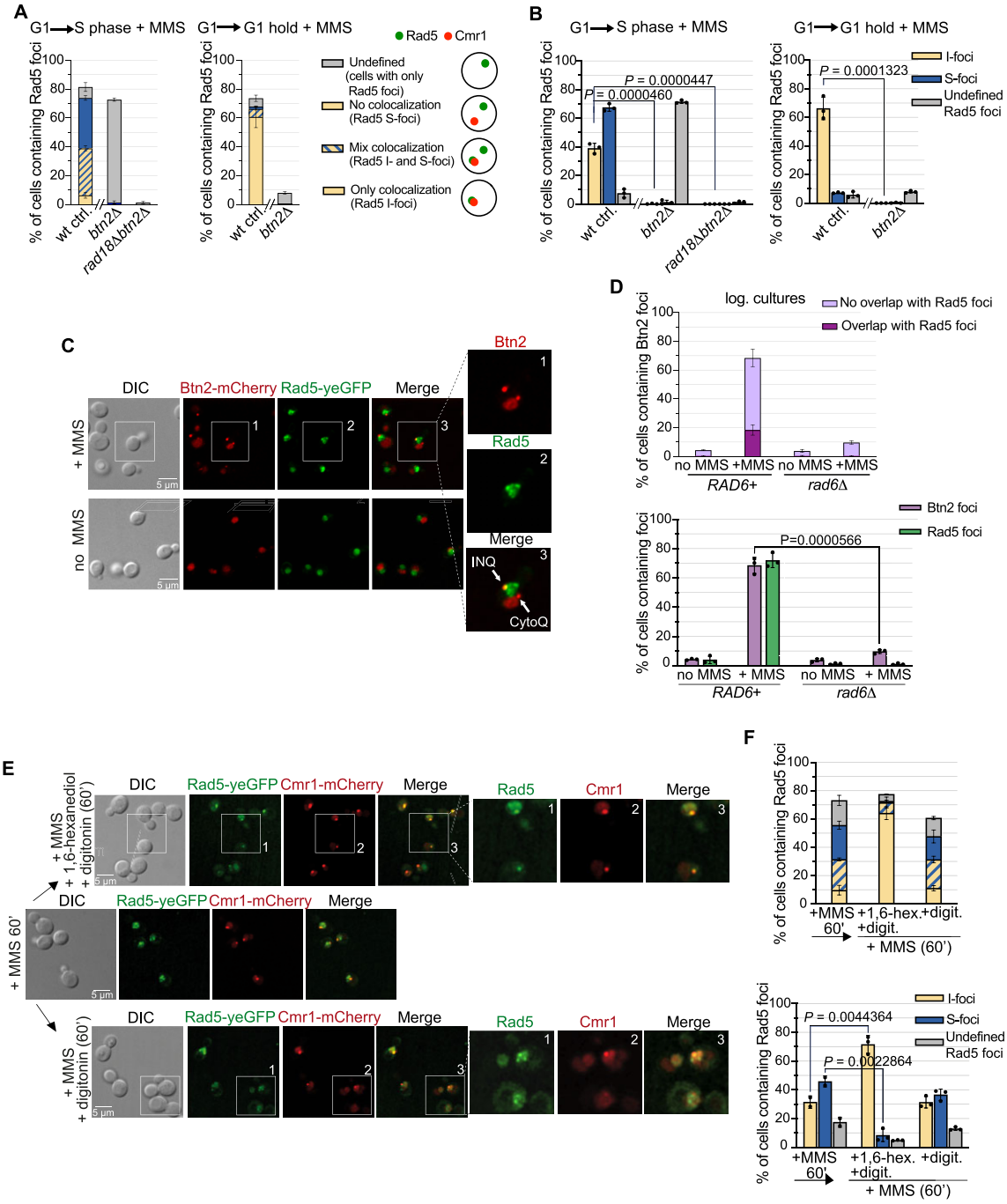


**Figure 3.** Rad5 is recruited into I- or S-foci by different mechanisms. (**A**, **B**) Btn2 is required for Rad5 I-foci formation. For S phase analysis (left panels), G1-synchronized cells were released into S phase in fresh medium (+0.033% MMS, 60 min) and analysed by fluorescence microscopy. For G1 analysis (right panels), cells were synchronized using α factor and held in G1 (+0.033% MMS, 60 min). (A) Data quantification of the fluorescence microscopy analysis. A diagram of the possible colocalization patterns between Rad5 and Cmr1 foci is shown. (B) Percentage of cells containing each type of Rad5 foci, calculated based on the total population of cells analysed using the data from (A). Statistical significance was calculated between the percentage of cells with Rad5 I-foci in the wild type-control and each mutant. wt-control data are the same as in Figure 2. Strains: wt-control (YCL51), *btn2*Δ (YCL148), *rad18*Δ*btn2*Δ (YCL198). (**C**, **D**) Btn2 forms foci that colocalize with Rad5 I-foci and depend on Rad6. Analysis of cycling cells (–/+0.033% MMS, 60 min). (C) Example photo of *RAD6*$^{+}$ cells. (D) Upper panel: data quantification of Btn2 foci and their colocalization with Rad5 foci. Lower panel: percentage of cells containing Btn2 or Rad5 foci in *RAD6* + or *rad6*Δ cells, calculated based on the total population of cells analysed using the data from the above panel. Statistical significance was calculated between the percentage of cells with Btn2-foci in *RAD6*+ and the *rad6*Δ mutant. Strains: *RAD5-yeGFP BTN2-mCherry* (YCL175), *rad6*Δ *RAD5-yeGFP BTN2-mCherry* (YCL208). (**E**, **F**) Rad5 S-foci are very likely formed by liquid-liquid phase separation. Cycling cells (*RAD5-yeGFP CMR1-mCherry*, YCL51 strain) were treated with 0.033% MMS, 60 min. The culture was then split in two and grown for an additional 60 min in the presence of 0.033% MMS, with the addition of 2.5% 1,6-hexanediol and 1 μg/ml digitonin, or just digitonin (control). (E) Example photos. (F) Upper panel: data quantification showing the percentage of cells containing each type of foci before and after hexanediol treatment. Lower panel: percentage of cells containing each type of Rad5 foci, calculated based on the total population of cells analysed using the data from the above panel. Statistical significance was calculated between the percentage of cells treated 60 min with 0.033% MMS containing Rad5 I- or S-foci and the corresponding Rad5 foci type after treatment or not with hexanediol. In all cases, the bar graphs represent the mean ± SD from three independent experiments. Only statistically significant *P* values ($P < 0.01$) are shown.

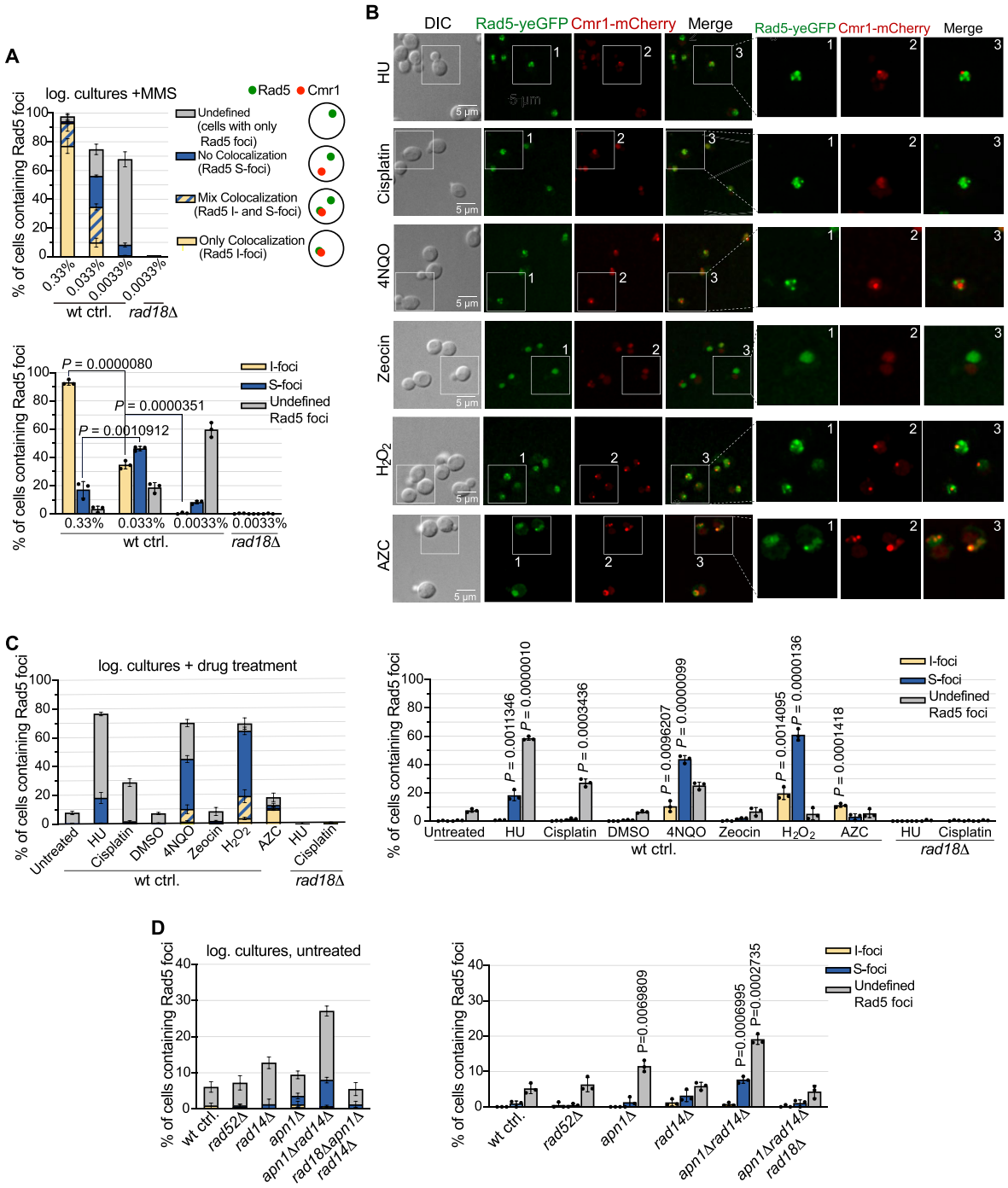


**Figure 4.** Rad5 S- and I- foci form in response to genotoxic and proteotoxic stress, respectively. (**A**) MMS dose affects Rad5 relocalization. Cycling cells were treated as indicated for 60 min and analysed by microscopy. Upper panel: percentage of cells containing each type of Rad5 foci. A diagram of the possible colocalization patterns between Rad5 and Cmr1 foci is shown. Lower panel: percentage of cells containing each type of Rad5 foci, calculated based on the total population of cells analysed using the data from the above panel. Statistical significance was calculated between the percentage of cells treated with 0.033% MMS containing Rad5 I- or S-foci and the corresponding Rad5 foci type of the other treatment conditions. Strains: wt-control (*RAD5-yeGFP CMR1-mCherry,* YCL51), *rad18Δ RAD5-yeGFP CMR1-mCherry* (YCL126). (**B**, **C**) Rad5 foci formation in response to different drugs. Cycling cells were treated for 60 min, except AZC (120 min) as follows: 200 mM HU, 0.5 mM cisplatin, 0.5 µg/ml 4NQO, 100 µg/ml zeocin, 0.4 mM $H_2O_2$, 1 mg/ml AZC. DMSO (solvent) is a control for cisplatin. Strains: YCL51, YCL126. (B) Example photos. (C) Left panel: quantification of Rad5 foci. Right panel: percentage of cells containing each type of Rad5 foci, calculated based on the total population of cells analysed using the data from the left panel. Statistical significance was calculated between the percentage of untreated cells containing I-foci, S-foci, or undefined Rad5-foci and the corresponding Rad5 foci type of the other treatment conditions. Strains: wt-control (*RAD5-yeGFP CMR1-mCherry,* YCL51), *rad18Δ RAD5-yeGFP CMR1-mCherry* (YCL126). (**D**) Analysis of spontaneous Rad5 foci in untreated DNA repair mutants. Cycling cells were analysed by fluorescence microscopy. Left panel: quantification of Rad5 foci. Right panel: percentage of cells containing each type of Rad5 foci, calculated based on the total population of cells analysed using the data from the left panel. Statistical significance was calculated between the percentage of cells with each type of Rad5 foci in the wild type-control and the corresponding Rad5 foci type of each mutant. Strains: wt-control (YCL51), *rad52Δ* (YCL199), *rad14Δ* (YCL183), *apn1Δ* (YCL131), *apn1Δ rad14Δ* (YCL202), *rad18Δ apn1Δ rad14Δ* (YCL239). In all cases, the bar graphs represent the mean ± SD from three independent experiments. Only statistically significant *P* values ($P < 0.01$) are shown.

Drugs expected to only affect DNA, such as cisplatin and hydroxyurea, induced only S-foci, confirmed by the elimination of undefined Rad5-foci when deleting *RAD18*; drugs that only affect proteins, such as the proline analogue azetidine-2-carboxylic acid (AZC), caused formation of only I-foci; drugs that, like MMS, affect both DNA and proteins, such as 4NQO and $H_2O_2$, induced I- and S-foci (Figure 4B, C and Supplementary Figure S4B). Therefore, a correlation exists between the type of cellular stress and the type of Rad5 foci formed. Importantly, drugs that induce S-foci cause problems that must be overcome by Rad5, as *rad5*Δ cells are sensitive to these compounds (56–58). These data show a direct link between Rad5-mediated tolerance of genotoxic stress and recruitment of this protein into S-foci, consistent with these being possible sites of protein activity. Moreover, the number of cells containing spontaneous S-foci significantly increased in a base excision repair and nucleotide excision repair double mutant, confirmed by the reduction of undefined Rad5-foci when deleting *RAD18* (Figure 4D and Supplementary Figure S4C), likely due to an accumulation of endogenous DNA damage. This additionally associates S-foci with genotoxic stress, whether of exogenous or endogenous origin.

## Rad5 S-foci are linked to sites of DDT function

The above data on S-foci, such as the requirement of a functional DDT pathway for their formation, their occurrence only during S-phase, and the fact that they are induced by genotoxic stress, suggest that these foci are related to Rad5 function. If this were the case, one might expect Rad5 S-foci to be spatially associated with proteins of the Rad6/Rad18 DDT pathway. As Rad18 is required for both the formation of S-foci and Rad5 function in DDT, we analysed the possible colocalization of Rad5 and Rad18. We found that, like Rad5, Rad18 also relocalized to foci in response to MMS treatment during S phase (Supplementary Figure S5A, B). Of note, Rad18 formed multiple foci per cell and, in a moderate number of cells, one of these foci colocalized with Cmr1 at the INQ (Supplementary Figure S5A, B). To examine whether the non-INQ Rad18 foci colocalize with Rad5 S-foci, we analysed colocalization between Rad18 and Rad5 in *btn2*Δ cells, which are unable to form INQ. We observed a high number of cells containing Rad18 foci that colocalized with Rad5 S-foci (Figure 5A, B), showing a spatial association of S-foci with the Rad6/Rad18 DDT pathway and thus supporting that they are related to Rad5 function.

To further study the spatial association of Rad5 with the DDT pathway, we investigated the possible colocalization of Rad5 S-foci with MMS-induced foci of Rfa1, the large subunit of RPA, since the coating of ssDNA by RPA following fork stalling is the signal to activate DDT (16). There was a high degree of overlap between Rad5 S-foci and Rfa1 foci after MMS treatment (Figure 5C, D), which supports that S-foci are related to DDT sites. It was shown recently that MMS-induced Rfa1-foci mark post-replicative repair territories (PORTs) (59), defined as clusters of ssDNA that arise from DNA polymerase blocking lesions in the wake of replication forks (59). Therefore, Rad5 might colocalize with Rfa1 behind replication forks, suggesting that S-foci represent post-replicative sites of DDT activity.

To continue the analysis of the potential link of S-foci with Rad5 function, we next studied whether these foci associate with sites of DNA damage where Rad5 would promote DNA lesion bypass (24,33,60,61). Rad5 and its human homologue HLTF require the HIRAN domain for binding to DNA and PCNA (61–64). A recently described Rad5 HIRAN mutant (*rad5-3RE*) disrupts protein binding to DNA *in vitro* and impedes MMS-induced Rad5-chromatin association (62). We found that MMS-treated *rad5-3RE* cells displayed complete absence of S-foci with no effect on I-foci (Figure 5E, F and Supplementary Figure S5C), supporting that S-foci are indeed sites where Rad5 accumulates and associates with damaged chromatin. Although the importance of the HIRAN domain for Rad5 foci formation was previously described (25), only a partial reduction in the number of HIRAN mutant cells with Rad5 foci had been observed. This partial reduction can now be explained by the existence of two types of Rad5 foci, given our result that the HIRAN domain is required for the formation of only S-foci but not I-foci. As the HIRAN domain is required for the binding of Rad5 to DNA, one would expect the response to DNA damage or replicative stress to be compromised in HIRAN mutants, despite the fact that overall protein folding is unaffected and they retain Rad5 activities (62,64). Accordingly, *rad5-3RE* cells are more sensitive to chronic treatment with MMS or HU than wild type cells (62). In a more specific analysis, we found that *rad5-3RE* cells underwent a steep viability drop when treated with MMS during a single S-phase (Figure 5G), which may correlate the presence of S-foci, where Rad5 is recruited following genotoxic stress, with the ability to tolerate DNA damage during chromosome replication.

Since Rad5 allows the bypass of unrepaired DNA lesions that interfere with the progression of replication forks, we also analysed the relevance of the Mec1/Rad53 checkpoint (ATR/Chk1, human functional homologues) for Rad5 relocalization, as this pathway prevents fork collapse in the presence of DNA damage or replicative stress (32,65,66). Recruitment of Rad5 into foci was barely affected in *mec1*Δ or *rad53*Δ mutants (Figure 5H and Supplementary Figure S5D), indicating that the S-phase checkpoint is not required for Rad5 relocalization and, in turn, that the establishment or maintenance of MMS-induced Rad5 S-foci do not rely on intact replication forks.

## I-foci represent sites of sequestration of non-functional Rad5 for subsequent refolding

I-foci are clearly different to S-foci, and the fact that their formation is modulated by Ubr2-mediated downregulation of Rpn4 points to a link with proteasome activity. Proteasome-mediated degradation is one of the mechanisms for coping with misfolded proteins, and thus a key component of the proteostasis network. Many proteins are recruited to the INQ after proteasome inhibition (34), but we found that while treatment with the proteasome inhibitor MG132 strongly induced Cmr1 foci, as shown before (34), there was little induction of Rad5 foci (Figure 6A and Supplementary Figure S6A). However, a combined treatment with MMS and MG132 caused a sharp increase in the number of cells with I-foci, but not S-foci, with respect to just MMS treatment (Figure 6A and Supplementary Figure S6A), suggesting that a significant fraction of MMS-damaged Rad5 molecules are sent to I-foci when they cannot be degraded by the proteasome.

Given that Rad6 is a negative modulator of the proteasome via Ubr2, we next investigated if the dependency on Rad6 for I-foci formation could be bypassed by proteasome inhibition.

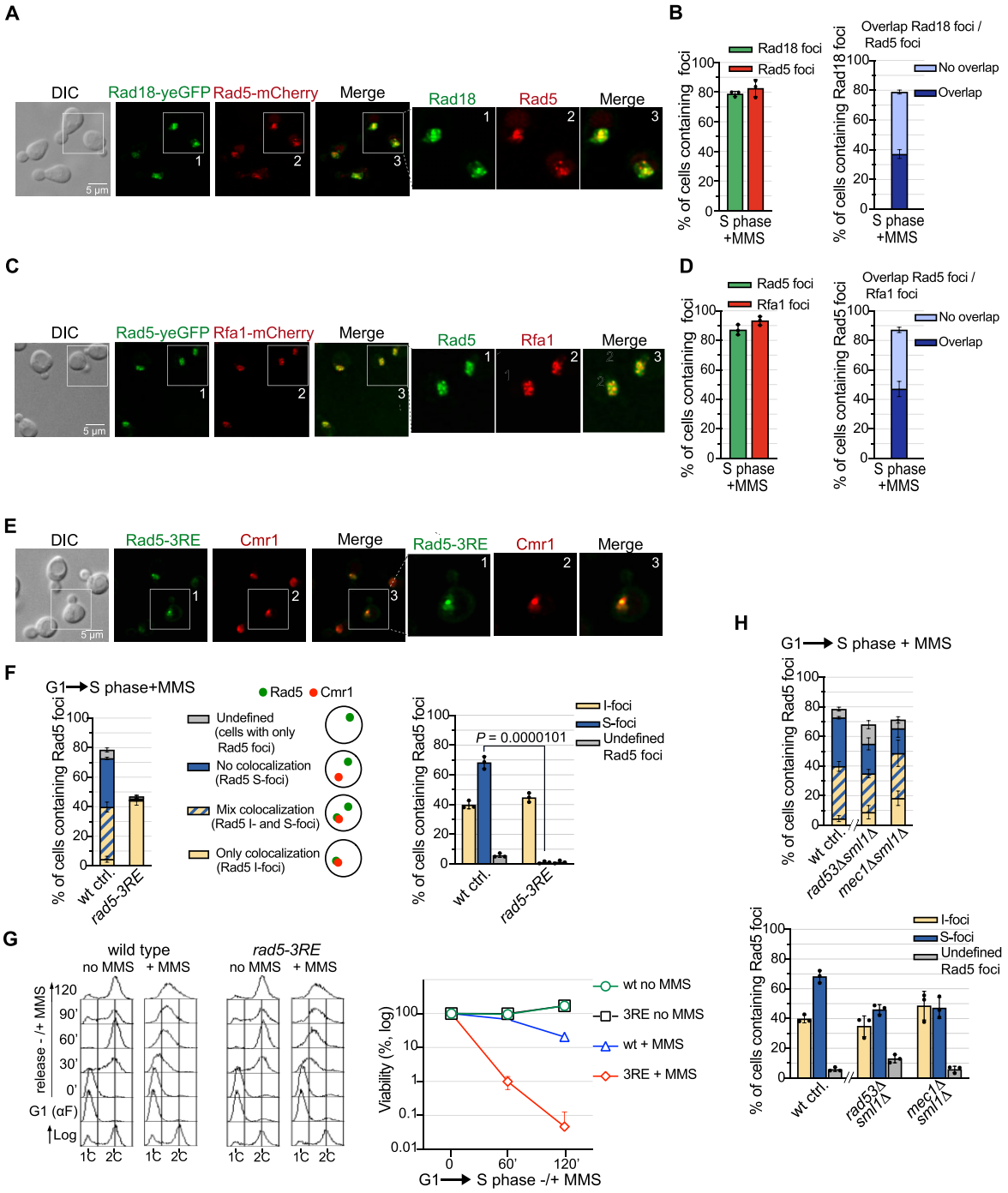


**Figure 5.** Rad5 S-foci are linked to sites of DDT function. (**A**, **B**) Colocalization of Rad5-foci and Rad18-foci in *btn2*Δ cells. G1-synchronized cells were released into S phase in fresh medium (+0.033% MMS, 60 min) and analysed by fluorescence microscopy. (A) Example photo. (B) Left panel: quantification of the number of cells containing Rad18-foci or Rad5-foci. Right panel: quantification of Rad5-foci overlap with Rad18-foci. Strain: *btn2*Δ *RAD18-yeGFP RAD5-mCherry* (YCL241). (**C**, **D**) Rad5 S-foci localize to PORTs. G1-synchronized cells were released into S phase (+MMS 0.033%, 60 min) and analysed by fluorescence microscopy. (C) Example photos. (D) Left panel: quantification of the number of cells containing Rad5-foci or Rfa-foci. Right panel: quantification of Rad5-foci overlap with Rfa1-foci. Strain: *RAD5-yeGFP RFA1-mCherry* (YCL57). (**E**, **F**) Rad5's HIRAN domain is required for S-foci formation. G1-synchronized cells were released into S phase (+MMS 0.033%, 60 min) and analysed by fluorescence microscopy. (E) Example photo. (F) Left panel: quantification of Rad5 foci. A diagram of the possible colocalization patterns between Rad5 and Cmr1 foci is shown. Right panel: percentage of cells containing each type of Rad5 foci, calculated based on the total population of cells analysed using the data from the left panel. Statistical significance was calculated between the percentage of cells with Rad5 I- or S-foci in the wild type-control and the corresponding Rad5 foci type of the *rad5-3RE* mutant. Strains: wt control (YCL51), *rad5-3RE-yeGFP* (YCL186). (**G**) Cell viability analysis. G1-synchronized cells were released into S phase (–/+ 0.033% MMS) to study cell viability. Left panel: cell cycle progression was monitored by flow cytometry. Right panel: sensitivity to MMS during S phase. Strains: YCL51, YCL186. (**H**) Rad5 foci formation does not require the S-phase checkpoint. G1-synchronized cells were released into S phase (+MMS 0.033%, 60 min) and analysed by fluorescence microscopy. Upper panel: quantification of Rad5 foci. wt-control data are as in (F). Lower panel: percentage of cells containing each type of Rad5 foci, calculated based on the total population of cells analysed using the data from the above panel. Strains: wt-control (YCL51), *rad53*Δ*sml1*Δ (YCL137), *mec1*Δ*sml1*Δ (YCL152). In all cases, the bar graphs or values represent the mean ± SD from three independent experiments. Only statistically significant *P* values ($P < 0.01$) are shown.

*rad6*Δ cells treated with MMS plus MG132 showed a strong rescue of Rad5 I-foci but not S-foci as compared to just MMS treatment (Figure 6A, B and Supplementary Figure S6A), indicating that proteasome inhibition by Rad6 is important for Rad5 recruitment into I-foci. The absence of Rad6 very likely leads to increased proteasome activity via elevated levels of Rpn4, and possibly via misregulated gene expression involving the Rad6/Bre1/histone H2B pathway.

Taking the above into account, we asked whether the absence of Rad5 foci in G2/M cells treated with MMS (Figure 1B and Supplementary Figure S1B) could be explained by proteasome activity. We found that proteasome inhibition by MG132 in MMS-treated G2/M arrested cells significantly induced the formation of Rad5 I-foci, but not S-foci (Figure 6C, D and Supplementary Figure S6B). This result indicates that in G2/M, unlike G1 or S phase, degradation of damaged or misfolded Rad5 via proteasome is strongly favoured over recruitment into I-foci. Moreover, protein recruitment to the INQ in G2/M appears to be hindered in general by proteasome activity, as we detected only a small number of MMS-treated G2/M cells containing Cmr1 foci, which increased very significantly after treatment with MG132 (Figure 6C, D and Supplementary Figure S6B).

Misfolded proteins at INQ can later be degraded or refolded, needing to be first disaggregated by two competing chaperones: Apj1 and Hsp104, which favour protein degradation and refolding, respectively (35,67). If it is indeed misfolded Rad5 that is recruited into I-foci, these might be disaggregated by one of these chaperones. We found that in wild-type control cells, both Rad5 S- and I-foci gradually resolved after MMS removal, correlating with S-phase progression, as shown by flow cytometry (Figure 6E, F and Supplementary Figure S6C). This shows that recruitment into I- and S-foci are reversible processes. In *apj1*Δ cells, Rad5 foci resolved similarly to the control, meaning Apj1 is not necessary for I-foci resolution and suggesting Rad5 at I-foci is not targeted for degradation. In stark contrast, Rad5 I-foci did not resolve in *hsp104*Δ cells (Figure 6E, F and Supplementary Figure S6C), indicating Hsp104 is essential for I-foci dissolution and in turn strongly suggesting Rad5 recruited into these foci can later be refolded into functional protein. Taken these and above data together, we propose I-foci represent sites of sequestered non-functional Rad5 for later refolding, indicating these foci play a role in protein homeostasis.

## Discussion

The Rad5/HLTF protein plays a central role in the tolerance to unrepaired DNA lesions during chromosome replication, and is therefore fundamental in the cellular response to DNA damage. In this work we have investigated the spatial regulation of *S. cerevisiae* Rad5 and found that its intranuclear relocalization into two types of nuclear foci under conditions of cellular stress is linked to both its function in DNA damage tolerance and its own homeostasis, exemplifying the interconnection between the networks involved in genome stability maintenance and proteostasis.

Our conclusion that Rad5 S-foci are related to the activity of this protein in DNA damage tolerance is supported by several data. Thus, S-foci formation occurs only during S phase, when Rad5 exerts its function, and requires a functional upstream DDT pathway, as it is dependent on PCNA monoubiquitylation by Rad6/Rad18. Also connecting Rad5 S-foci to DDT is their colocalization with both DNA damage-induced Rad18- and Rfa1-foci. Another correlation between S-foci and DDT function is that they form not only in response to MMS, but also after treatment with different drugs that cause genotoxic stress and lead to problems that must be overcome by Rad5 (56–58), as well as in mutants that accumulate endogenous DNA damage.

Importantly, formation of S-foci, but not I-foci, requires the HIRAN domain of Rad5. The requirement of this domain for Rad5 association with chromatin under conditions of DNA damage (62) supports that S-foci represent sites of Rad5 recruitment to damaged chromatin. In addition, the correlation between the absence of S-foci in *rad5*-HIRAN mutant cells and the loss of viability they undergo after MMS treatment during a single S-phase is consistent with these foci being important for Rad5 function. In this regard, while Rad5 HIRAN mutants retain ubiquitylation activity *in vitro* (62,64), the marked reduction in their ability to polyubiquitylate PCNA *in vivo* (62) may be explained by the inability of the Rad5-HIRAN mutant to form S-foci and thus to accumulate at the sites of DNA lesions, which would hinder its interaction with PCNA. In turn, this failure in PCNA polyubiquitylation could explain the impossibility of a subsequent function of the protein in DDT even though Rad5 HIRAN mutants maintain proper folding and activities (62,64), which would account for the loss of cell viability after MMS treatment in *rad5-HIRAN* mutant cells.

Our results indicate that Rad5 S-foci, but not I-foci, are very likely formed by liquid-liquid phase separation. Phase separation of Rad5 into liquid-like condensates could help the protein to transiently concentrate at sites of DNA lesions. As Rad5 S-foci formation is dependent on PCNA monoubiquitylation, it may be that this modification is the nucleation event that triggers Rad5 protein phase separation to form this type of foci. It is also possible that the HIRAN domain is involved in this process, as the potential of some proteins to phase separate *in vivo* depends on their ability to bind DNA (68). Regarding the resolution of Rad5 S-foci, our data show that they are not the final fate of the protein but rather dissolve gradually after MMS removal and in concert with the completion of chromosome replication, suggesting that they disaggregate after Rad5 has completed its function in DDT.

Unlike Rad5 S-foci, Rad5 I-foci are not directly related to Rad5 function, but instead we propose they represent sites of recruitment of damaged or misfolded Rad5 associated with the quality control of this protein. This conclusion was initially based on: (i) I-foci formation does not depend on a functional *RAD6/RAD18* DDT pathway; (ii) I-foci colocalize with INQ compartments; (iii) I-foci form when cells are treated with agents that result in proteotoxic stress, regardless of whether, like MMS, they also cause genotoxic stress, but not with those that only affect DNA. Concerning MMS, this model drug is widely used as, and considered to be, a compound that causes DNA damage, with little concern for the fact that it can also damage proteins, possibly triggering their misfolding (53–55). Our data strongly suggest that it would not be the genotoxic effect of MMS that induces the relocalization of the protein to I-foci, but the proteotoxic stress that acts directly on Rad5.

While the formation of I-foci, like S-foci, is driven by Rad6, relocalization of Rad5 to the former involves pathways outside of Rad6/Rad18 DDT. Thus, recruitment of Rad5 into I-foci requires both Rad6/Ubr2/Rpn4 and Rad6/Bre1/histone

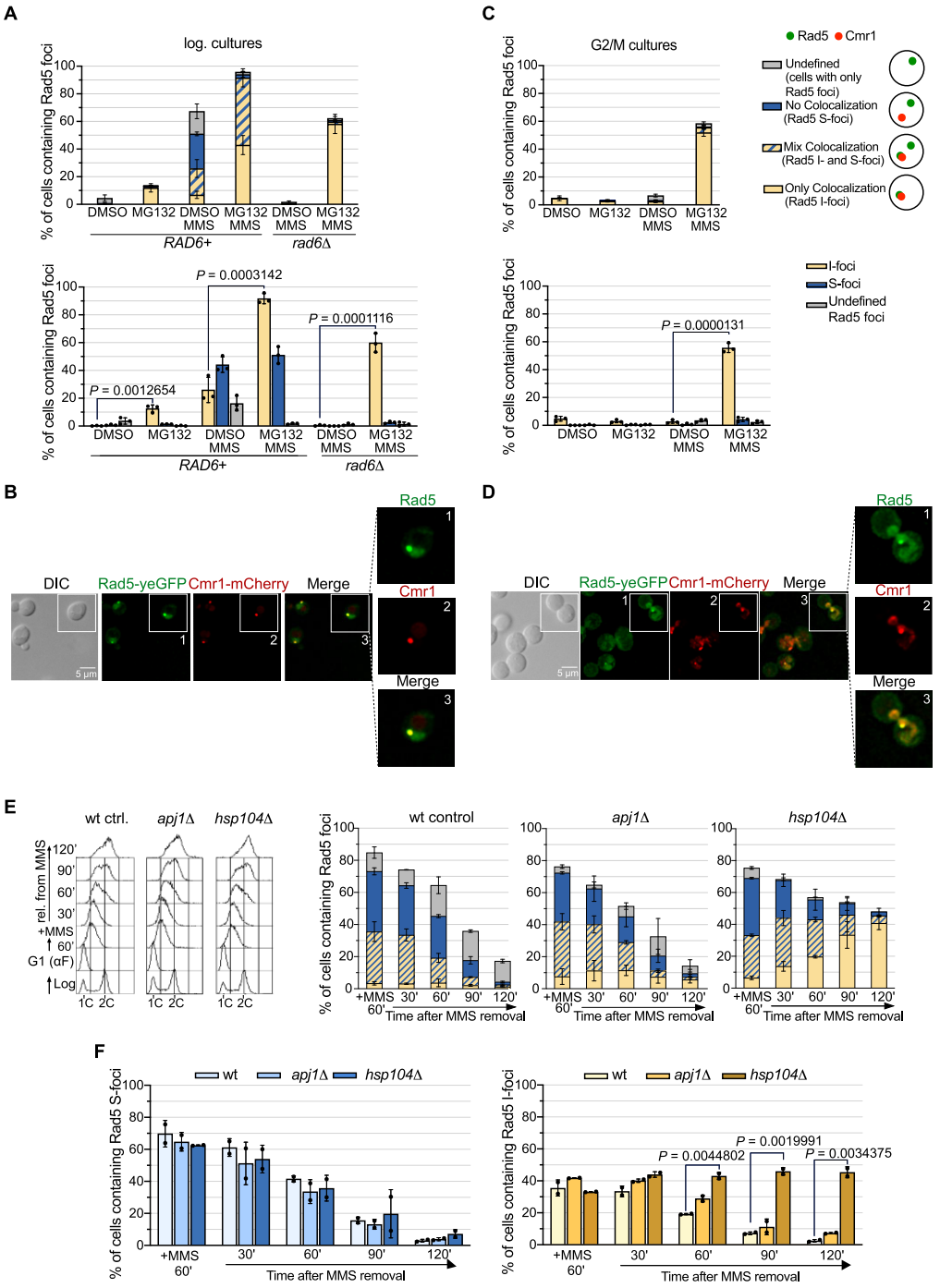


**Figure 6.** I-foci are sites of recruitment of non-functional Rad5 for later refolding. (**A**, **B**) Combined MMS and MG132 treatment increases Rad5 I-foci and bypasses the Rad6 dependency. Cycling cells were treated for 60 min with either 0.033% MMS, 75 μg/ml MG132, or both. DMSO (solvent) is a control for MG132. (A) Upper panel: quantification of Rad5 foci. A diagram of the possible colocalization patterns between Rad5 and Cmr1 foci is shown on the far right of the Figure. Lower panel: percentage of cells containing each type of Rad5 foci, calculated based on the total population of cells analysed using the data from the upper panel. Statistical significance between the number of cells with I-foci comparing relevant treatment conditions is shown. (B) Example photo of *rad6*Δ cells treated with MMS + MG132. Strains: wt-control (YCL51), *rad6*Δ (YCL149). (**C**, **D**) Combined MMS and MG132 treatment allows for formation of Rad5 I-foci during G2/M phase. G2/M synchronized cells were treated for 60 min with either 0.033% MMS, 75 μg/ml MG132, or both. DMSO (solvent) is a control for MG132. (C) Upper panel: quantification of Rad5 foci. Lower panel: percentage of cells containing each type of Rad5 foci, calculated based on the total population of cells analysed using the data from the upper panel. Statistical significance between the number of cells with I-foci comparing relevant treatment conditions is shown. (D) Example photo of G2/M cells treated with MMS + MG132. Strain: YCL51. (**E, F**) Rad5-foci resolution time course. I-foci resolution requires the Hsp104 disaggregase. G1-synchronized cells were released into S phase (+0.033% MMS, 60 min). MMS was removed and cells were allowed to progress in S phase for 120 min, monitored by flow cytometry (E, left panel), with samples taken for microscopy analysis. Right panel: quantification of the percentage of cells with each type of Rad5 foci during the experiment. (F) Left panel: percentage of cells containing Rad5 S-foci. Right panel: percentage of cells containing Rad5 I-foci. All percentages were calculated based on the total population of cells analysed using the data from (E). Relevant *P* values are shown. Strains: wt-control (YCL51), *apj1*Δ (YCL212), *hsp104*Δ (YCL165). The experiment was conducted in duplicate. The bar graphs represent the mean ± SD from three independent experiments. Relevant *P* values are shown.

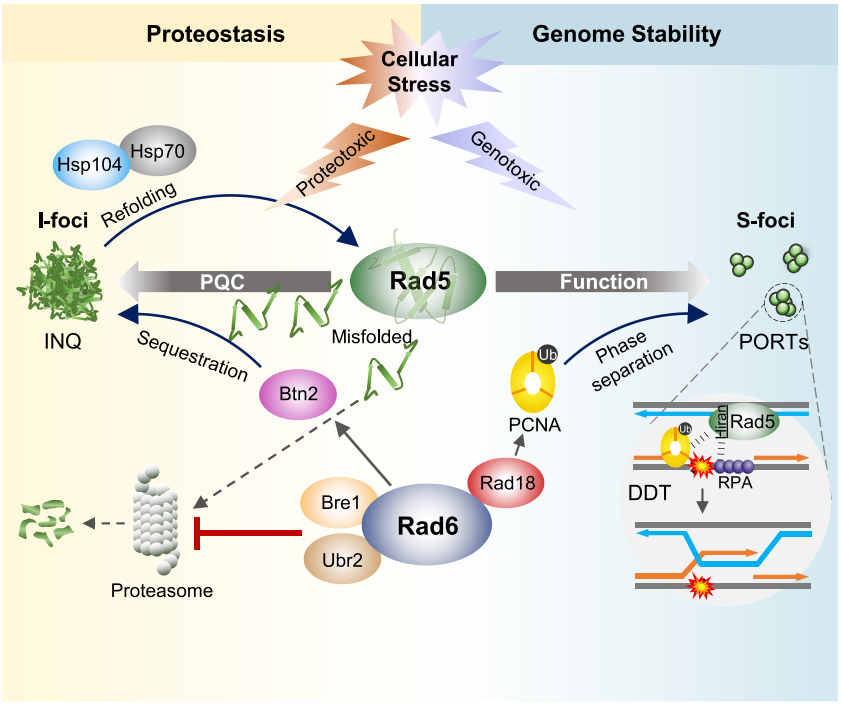


**Figure 7.** Model for spatial regulation of DNA damage tolerance protein Rad5 in response to MMS-induced cellular stress. The alkylating compound MMS causes both genotoxic and proteotoxic stress, and its use as a model stress agent shows that subnuclear relocalization of Rad5 is important for both genome and proteome stability. We propose a model for MMS-induced recruitment of Rad5 into foci, with Rad6 as a key factor interconnecting genome stability maintenance and proteostasis networks. MMS-induced DNA lesions force replication forks to stall. Many stalled forks are overcome by re-priming, which leaves behind ssDNA gaps that are covered by RPA and recruited to post-replicative territories (PORTs). RPA triggers DDT by recruitment of Rad6/Rad18 to monoubiquitylate PCNA. This in turn causes Rad5 relocalization into S-foci at the PORTs via a process likely involving liquid-liquid phase separation and recognition of PCNA and/or ssDNA by the Rad5 HIRAN domain. Recruitment of Rad5 into S-foci would favour Rad5-mediated template switching to fill in ssDNA gaps, allowing cells to complete chromosome replication. However, some Rad5 molecules are also damaged and misfolded by MMS. Rad6 here acts via the Rad6/Bre1/histoneH2B and Rad6/Ubr2/Rpn4 pathways to downregulate the proteasome, and through the Btn2 sequestrase to recruit damaged/misfolded Rad5 into I-foci at the INQ compartment. This process favours protein quality control by avoiding non-functional Rad5 at sites of DNA damage while preventing its degradation. Non-functional Rad5 recruited at I-foci can later be refolded via the Hsp104/Hsp70 chaperone system into functional Rad5 that would then be available to carry out DNA damage tolerance.

H2B pathways. The involvement of the former in Rad5 I-foci formation suggests that protein recruitment into these foci is modulated by proteasome activity. This idea is reinforced by the fact that exogenous proteasome inhibition increases MMS-induced recruitment of Rad5 into I-foci, suggesting that the MMS damages the protein, resulting in some of the molecules being degraded by the proteasome while others are recruited into I-foci, with proteasome activity deciding the balance between these two fates. This conclusion is further supported by our data that exogenous proteasome inhibition in *rad6*Δ MMS-treated cells is sufficient to rescue the formation of Rad5 I-foci, but not S-foci, as well as by the result that in G2/M cells treated with MMS, which do not show foci, proteasome inhibition induces the formation of Rad5 I-foci. The latter suggests that, once cells have reached prometaphase, recruitment of damaged or misfolded proteins into this type of foci may not be beneficial for the cell and, instead, these proteins are targeted for degradation. Moreover, the fact that only Rad5 I-foci are formed when the proteasome is inhibited in MMS-treated G2/M cells is consistent with S-foci being associated with chromosome replication. Given that Rad6/Bre1-dependent histone H2B ubiquitylation is also important for Rad5 recruitment into I-foci, we believe it is possible that Rad6/Bre1 may also influence the expression of proteasome-related genes, contributing together with Rad6/Ubr2 to downregulate proteasome activity and favour Rad5 relocalization into I-foci. We propose a model whereby misfolded or damaged Rad5 can be recruited into I-foci or degraded by the proteasome, with Rad6, through two complementary pathways, being a key factor that decides the fate of Rad5.

The dynamics of formation and disaggregation of Rad5 I-foci, driven respectively by the Btn2 sequestrase and the Hsp104 chaperone, is consistent with the idea they are composed of misfolded or damaged Rad5 molecules. Btn2 is not only required for I-foci formation but also relocalizes like Rad5 to INQ, which is necessary for its function in protein sequestration (44). We showed that Rad6 is required for Btn2 recruitment into these foci, indicating that it is a key regulator of this chaperone. Interestingly, Btn2 foci form following proteasome inhibition (34), and Btn2 protein levels are stabilized by both proteasome inhibition and MMS treatment (10). It is therefore possible that the modulatory effect of Rad6 on proteasome activity contributes to relocalization of Rad5 into I-foci not only by inhibiting degradation of Rad5, but also by favouring the accumulation of Btn2 to the levels required for this chaperone to be recruited to INQ and carry out its sequestrase function. Like S-foci, I-foci are not the final destination of Rad5, as they disaggregate once the cellular stress disappears. Notably, I-foci resolution requires Hsp104, which facilitates protein refolding, and not Apj1, which favours protein degradation (35,67). Together with the above, these data

strongly suggest that misfolded Rad5 is recruited into I-foci as an alternative to proteasome degradation and that the whole process occurs to ultimately favour refolding of misfolded Rad5 protein, indicating a proteostasis function for I-foci. Recruitment into I-foci might protect cells from the potential toxicity of misfolded Rad5, or it may simply function as a filter to favour the recruitment of unadulterated protein into S-foci, thereby ensuring that only functional Rad5 is recruited to sites of DDT. Protein refolding after recruitment into I-foci instead of degradation may be advantageous for maintaining high levels of functional Rad5 in the presence of continued cellular stress, which would ensure efficient DNA damage tolerance activity. Future studies will be necessary to analyse how Rad5 can refold after being damaged and sequestered, as well as to decipher the exact contribution of this process to DNA damage tolerance.

Beyond the importance for the function and homeostasis of the DNA damage tolerance protein Rad5, its spatial regulation in response to cellular stress by recruitment into two different types of coexisting nuclear foci provides a model to illustrate the interconnection between genome stability maintenance and proteostasis networks (Figure 7). This model in turn helps to understand cellular homeostasis as a whole. As explained, the differential relocalization of Rad5 into S- or I-foci is linked through a common dependency on Rad6, which emerges as a key protein connecting different networks necessary to preserve cellular homeostasis (Figure 7). We believe these findings have important implications for future studies analysing protein relocalization and other cellular stress responses, as many sources of stress, on their own or in combination, can affect both DNA and proteins. This is particularly relevant for studies on the cellular response to DNA damage, as the observed phenotypes due to exposure to different agents may be due not only to DNA lesions, but also to non-functional DNA damage response proteins caused by the proteotoxic stress. Of note, several diseases, such as cancer and neurodegenerative disorders, are associated with a combination of both genome and proteome instability (4,5), which we consider advantageous to study together for a deeper understanding of the underlying pathological processes. It would also be important to be mindful of medical treatments that could affect both DNA and proteins, such as those used in some cancer therapies.

## Data availability

The data underlying this work are available in the article and its online supplementary material. All materials are available upon request.

## Supplementary data

Supplementary Data are available at NAR Online.

## Acknowledgements

We thank Crisanto Gutiérrez (CBMSO) for critical reading of the manuscript, Xiaolan Zhao (Memorial Sloan Kettering Cancer Center, NY, USA) for the *rad5-3RE* HIRAN mutant, P. San Segundo (IBFG, Salamanca, Spain) for the *pol30K164R* mutant, Félix Prado (CABIMER, Seville, Spain) for the pFA6-mCherry (*NATMX6*) plasmid, Karim Labib (MRC, Univ. of Dundee, UK) for the *SPC42-egFP* strain, Helle Ulrich (IMB, Mainz, Germany) for the pFA6a-*URA3* plasmid and José María Requena (CBMSO) for the anti-mCherry antibody. We also thank Irene Saugar for her help in the first steps of this project and the Optical and Confocal Microscopy Facility of CBMSO for technical support.

## Funding

Spanish Ministry of Science and Innovation (MICINN) [PID2020-119708GB-I00 to J.A.T.]; C.P.L. is the recipient of a predoctoral fellowship (FPU) from MICINN; P.G.-F. is the recipient of a predoctoral fellowship (FPI) from MICINN; the CBMSO receives institutional grants from Fundación Ramón Areces and Banco Santander.

## Conflict of interest statement

None declared.

## References

1. Aguilera,A. and García-Muse,T. (2013) Causes of genome instability. *Annu. Rev. Genet.*, **47**, 1–32.
2. Zeman,M.K. and Cimprich,K.A. (2014) Causes and consequences of replication stress. *Nat. Cell. Biol.*, **16**, 2–9.
3. Hipp,M.S., Kasturi,P. and Hartl,F.U. (2019) The proteostasis network and its decline in ageing. *Nat. Rev. Mol. Cell Biol.*, **20**, 421–435.
4. Huiting,W. and Bergink,S. (2021) Locked in a vicious cycle: the connection between genomic instability and a loss of protein homeostasis. *Genome Instab. Dis.*, **2**, 1–23.
5. Schumacher,B., Pothof,J., Vijg,J. and Hoeijmakers,J.H.J. (2021) The central role of DNA damage in the ageing process. *Nature*, **592**, 695–703.
6. Ciccia,A. and Elledge,S.J. (2010) The DNA damage response: making it safe to play with knives. *Mol. Cell*, **40**, 179–204.
7. Balch,W.E., Morimoto,R.I., Dillin,A. and Kelly,J.W. (2008) Adapting proteostasis for disease intervention. *Science*, **319**, 916–919.
8. Tkach,J.M., Yimit,A., Lee,A.Y., Riffle,M., Costanzo,M., Jaschob,D., Hendry,J.A., Ou,J., Moffat,J., Boone,C., *et al.* (2012) Dissecting DNA damage response pathways by analysing protein localization and abundance changes during DNA replication stress. *Nat. Cell Biol.*, **14**, 966–976.
9. Lisby,M., Barlow,J.H., Burgess,R.C. and Rothstein,R. (2004) Choreography of the DNA damage response: spatiotemporal relationships among checkpoint and repair proteins. *Cell*, **118**, 699–713.
10. Miller,S.B., Ho,C., Winkler,J., Khokhrina,M., Neuner,A., Mohamed,M.Y., Guilbride,D.L., Richter,K., Lisby,M., Schiebel,E., *et al.* (2015) Compartment-specific aggregases direct distinct nuclear and cytoplasmic aggregate deposition. *EMBO J.*, **34**, 778–797.
11. Sontag,E.M., Samant,R.S. and Frydman,J. (2017) Mechanisms and functions of spatial protein quality control. *Annu. Rev. Biochem.*, **86**, 97–122.
12. Branzei,D. and Psakhye,I. (2016) DNA damage tolerance. *Curr. Opin. Cell Biol.*, **40**, 137–144.
13. Saugar,I., Ortiz-Bazán,M.A. and Tercero,J.A. (2014) Tolerating DNA damage during eukaryotic chromosome replication. *Exp. Cell Res.*, **329**, 170–177.
14. Ulrich,H.D. and Walden,H. (2010) Ubiquitin signalling in DNA replication and repair. *Nat. Rev. Mol. Cell. Biol.*, **11**, 479–489.
15. Sale,J.E. (2012) Competition, collaboration and coordination – determining how cells bypass DNA damage. *J. Cell Sci.*, **125**, 1633–1643.

16. Davies,A.A., Huttner,D., Daigaku,Y., Chen,S. and Ulrich,H.D. (2008) Activation of ubiquitin-dependent DNA damage bypass is mediated by replication protein A. *Mol. Cell*, **29**, 625–636.
17. Hoege,C., Pfander,B., Moldovan,G.L., Pyrowolakis,G. and Jentsch,S. (2002) RAD6-dependent DNA repair is linked to modification of PCNA by ubiquitin and SUMO. *Nature*, **419**, 135–141.
18. Stelter,P. and Ulrich,H.D. (2003) Control of spontaneous and damage-induced mutagenesis by SUMO and ubiquitin conjugation. *Nature*, **425**, 188–191.
19. Sale,J.E. (2013) Translesion DNA synthesis and mutagenesis in eukaryotes. *Cold Spring Harb. Perspect. Biol.*, **5**, a012708.
20. Unk,I., Hajdu,I., Blastyak,A. and Haracska,L. (2010) Role of yeast Rad5 and its human orthologs, HLTF and SHPRH in DNA damage tolerance. *DNA Repair Amst.*, **9**, 257–267.
21. Gallo,D., Kim,T., Szakal,B., Saayman,X., Narula,A., Park.,Y., Branzei,D., Zhang,Z. and Brown,G.W. (2019) Rad5 recruits error-prone DNA polymerases for mutagenic repair of ssDNA gaps on undamaged templates. *Mol. Cell*, **73**, 900–914.
22. Pages,V., Bresson,A., Acharya,N., Prakash,S., Fuchs,R.P. and Prakash,L. (2008) Requirement of Rad5 for DNA polymerase zeta-dependent translesion synthesis in *Saccharomyces cerevisiae*. *Genetics*, **180**, 73–82.
23. Xu,X., Lin,A., Zhou,C., Blackwell,S.R., Zhang,Y., Wang,Z., Feng,Q., Guan,R., Hanna,M.D., Chen,Z., *et al.* (2016) Involvement of budding yeast Rad5 in translesion DNA synthesis through physical interaction with Rev1. *Nucleic Acids Res.*, **44**, 5231–5245.
24. Ortiz-Bazán,M.A., Gallo-Fernández,M., Saugar,I., Jiménez-Martín,A., Vázquez,M.V. and Tercero,J.A. (2014) Rad5 plays a major role in the cellular response to DNA damage during chromosome replication. *Cell Rep.*, **9**, 460–468.
25. Fan,Q., Xu,X., Zhao,X., Wang,Q., Xiao,W., Guo,Y. and Fu,Y.V. (2018) Rad5 coordinates translesion DNA synthesis pathway by recognizing specific DNA structures in *Sacharomyces cerevisiae*. *Curr. Genet.*, **64**, 889–899.
26. Longtine,M.S., McKenzie,A., Demarini,D.J., Shah,N.G., Wach,A., Brachat,A., Philippsen,P. and Pringle,J.R. (1998) Additional modules for versatile and economical PCR-based gene deletion and modification in *Saccharomyces cerevisiae*. *Yeast*, **14**, 953–961.
27. Saugar,I., Jiménez-Martín,A. and Tercero,J.A. (2017) Subnuclear relocalization of structure-specific endonucleases in response to DNA damage. *Cell Rep.*, **20**, 1553–1562.
28. Sikorski,R.S. and Hieter,P. (1989) A system of shuttle vectors and yeast host strains designed for efficient manipulation of DNA in *Saccharomyces cerevisiae*. *Genetics*, **122**, 19–27.
29. Janke,C., Magiera,M.M., Rathfelder,N., Taxis,C., Reber,S., Maekawa,H., Moreno-Borchart,A., Doenges,G., Schwob,E., Schiebel,E., *et al.* (2004) A versatile toolbox for PCR-based tagging of yeast genes: new fluorescent proteins, more markers and promoter substitution cassettes. *Yeast*, **21**, 947–962.
30. Labib,K., Diffley,J.F.X. and Kearsey,S.E. (1999) G1-phase and B-type cyclins exclude the DNA-replication factor Mcm4 from the nucleus. *Nat. Cell Biol.*, **1**, 415–422.
31. Foiani,M., Marini,F., Gamba,D., Lucchini,G. and Plevani,P. (1994) The B subunit of the DNA polymerase alpha-primase complex in *Saccharomyces cerevisiae* executes an essential function at the initial stage of DNA replication. *Mol. Cell. Biol.*, **14**, 923–933.
32. Tercero,J.A. and Diffley,J.F. (2001) Regulation of DNA replication fork progression through damaged DNA by the Mec1/Rad53 checkpoint. *Nature*, **412**, 553–557.
33. Minca,E.C. and Kowalski,D. (2010) Multiple Rad5 activities mediate sister chromatid recombination to bypass DNA damage at stalled replication forks. *Mol. Cell*, **38**, 649–661.
34. Gallina,I., Colding,C., Henriksen,P., Beli,P., Nakamura,K., Offman,J., Mathiasen,D.P., Silva,S., Hoffmann,E., Groth,A., *et al.* (2015) Cmr1/WDR76 defines a nuclear genotoxic stress body linking genome integrity and protein quality control. *Nat. Commun.*, **6**, 6533.
35. Ho,C., Grousl,T., Shatz,O., Jawed,A., Ruger-Herreros,C., Semmelink,M., Zahn,R., Richter,K., Bukau,B. and Mogk,A. (2019) Cellular sequestrases maintain basal Hsp70 capacity ensuring balanced proteostasis. *Nat. Commun.*, **10**, 4851.
36. Kumar,A., Mathew,V. and Stirling,P.C. (2022) Nuclear protein quality control in yeast: the latest INQuiries. *J. Biol. Chem.*, **298**, 102199.
37. Ulrich,H.D. and Jentsch,S. (2000) Two RING finger proteins mediate cooperation between ubiquitin-conjugating enzymes in DNA repair. *EMBO J.*, **19**, 3388–3397.
38. Bailly,V., Lamb,J., Sung,P., Prakash,S. and Prakash,L. (1994) Specific complex formation between yeast RAD6 and RAD18 proteins: a potential mechanism for targeting RAD6 ubiquitin-conjugating activity to DNA damage sites. *Genes Dev.*, **8**, 811–820.
39. Dohmen,R.J., Madura,K., Bartel,B. and Varshavsky,A. (1991) The N-end rule is mediated by the UBC2(RAD6) ubiquitin-conjugating enzyme. *Proc. Natl. Acad. Sci. U.S.A.*, **88**, 7351–7355.
40. Wang,L., Mao,X., Ju,D. and Xie,Y. (2004) Rpn4 Is a physiological substrate of the Ubr2 ubiquitin ligase. *J. Biol. Chem.*, **279**, 55218–55223.
41. Wood,A., Krogan,N.J., Dover,J., Schneider,J., Heidt,J., Boateng,M.A., Dean,K., Golshani,A., Zhang,Y., Greenblatt,J.F., *et al.* (2003) Bre1, an E3 ubiquitin ligase required for recruitment and substrate selection of Rad6 at a promoter. *Mol. Cell*, **11**, 267–274.
42. Deng,Z.-H., Ai,H.-S., Lu,C.-P. and Li,J.-B. (2020) The Bre1/Rad6 machinery: writing the central histone ubiquitin mark on H2B and beyond. *Chromosome Res.*, **28**, 247–258.
43. Kruegel,U., Robison,B., Dange,T., Kahlert,G., Delaney,J.R., Kotireddy,S., Tsuchiya,M., Tsuchiyama,S., Murakami,C.J., Schleit,J., *et al.* (2011) Elevated proteasome capacity extends replicative lifespan in *Saccharomyces cerevisiae*. *PLoS Genet.*, **7**, e1002253.
44. Malinovska,L., Kroschwald,S., Munder,M.C., Richter,D. and Alberti,S. (2012) Molecular chaperones and stress-inducible protein-sorting factors coordinate the spatiotemporal distribution of protein aggregates. *Mol. Biol. Cell*, **23**, 3041–3056.
45. Banani,S.F., Lee,H.O., Hyman,A.A. and Rosen,M.K. (2017) Biomolecular condensates: organizers of cellular biochemistry. *Nat. Rev. Mol. Cell Biol.*, **18**, 285–298.
46. Boeynaems,S., Alberti,S., Fawzi,N.L., Mittag,T., Polymenidou,M., Rousseau,F., Schymkowitz,J., Shorter,J., Wolozin,B., Van Den Bosch,L., *et al.* (2018) Protein phase separation: a new phase in cell biology. *Trends Cell Biol.*, **28**, 420–435.
47. Oshidari,R., Huang,R., Medghalchi,M., Tse,E.Y.W., Ashgriz,N., Lee,H.O., Wyatt,H. and Mekhail,K. (2020) DNA repair by Rad52 liquid droplets. *Nat. Commun.*, **11**, 695.
48. Sabari,B.R., Dall'Agnese,A., Boija,A., Klein,I.A., Coffey,E.L., Shrinivas,K., Abraham,B.J., Hannett,N.M., Zamudio,A.V., Manteiga,J.C., *et al.* (2018) Coactivator condensation at super-enhancers links phase separation and gene control. *Science*, **361**, eaar3958.
49. Zhang,F., Biswas,M., Massah,S., Lee,J., Lingadahalli,S., Wong,S., Wells,C., Foo,J., Khan,N., Morin,H., *et al.* (2023) Dynamic phase separation of the androgen receptor and its coactivators key to regulate gene expression. *Nucleic Acids Res.*, **51**, 99–116.
50. Lin,Y., Mori,E., Kato,M., Xiang,S., Wu,L., Kwon,I. and McKnight,S.L. (2016) Toxic PR poly-dipeptides encoded by the C9orf72 repeat expansion target LC domain polymers. *Cell*, **167**, 789–802.
51. Nair,S.J., Yang,L., Meluzzi,D., Oh,S., Yang,F., Friedman,M.J., Wang,S., Suter,T., Alshareedah,I., Gamliel,A., *et al.* (2019) Phase separation of ligand-activated enhancers licenses cooperative chromosomal enhancer assembly. *Nat. Struct. Mol. Biol.*, **26**, 193–203.
52. Beranek,D.T. (1990) Distribution of methyl and ethyl adducts following alkylation with monofunctional alkylating agents. *Mutat. Res.*, **231**, 11–30.

53. Boffa,L.C. and Bolognesi,C. (1985) Methylating agents: their target amino acids in nuclear proteins. *Carcinogenesis*, **6**, 1399–1401.
54. Gasch,A.P., Huang,M., Metzner,S., Botstein,D., Elledge,S.J. and Brown,P.O. (2001) Genomic expression responses to DNA-damaging agents and the regulatory role of the yeast ATR homolog Mec1p. *Mol. Biol. Cell*, **12**, 2987–3003.
55. Jones,R.D. and Gardner,R.G. (2016) Protein quality control in the nucleus. *Curr. Opin. Cell Biol.*, **40**, 81–89.
56. Birrell,G.W., Brown,J.A., Wu,H.I., Giaever,G., Chu,A.M., Davis,R.W. and Brown,J.M. (2002) Transcriptional response of *Saccharomyces cerevisiae* to DNA-damaging agents does not identify the genes that protect against these agents. *Proc. Natl. Acad. Sci. U.S.A.*, **99**, 8778–8783.
57. Chang,M., Bellaoui,M., Boone,C. and Brown,G.W. (2002) A genome-wide screen for methyl methanesulfonate-sensitive mutants reveals genes required for S phase progression in the presence of DNA damage. *Proc. Natl. Acad. Sci. U.S.A.*, **99**, 16934–16939.
58. Jiménez-Martín,A., Saugar,I., Joseph,C.R., Mayer,A., Lehmann,C.P., Szakal,B., Branzei,D. and Tercero,J.A. (2020) The Mgs1/WRNIP1 ATPase is required to prevent a recombination salvage pathway at damaged replication forks. *Sci. Adv.*, **6**, eaaz3327.
59. Wong,R.P., García-Rodríguez,N., Zilio,N., Hanulová,M. and Ulrich,H.D. (2020) Processing of DNA polymerase-blocking lesions during genome replication is spatially and temporally segregated from replication forks. *Mol. Cell*, **77**, 3–16.
60. Giannattasio,M., Zwicky,K., Follonier,C., Foiani,M., Lopes,M. and Branzei,D. (2014) Visualization of recombination-mediated damage bypass by template switching. *Nat. Struct. Mol. Biol.*, **21**, 884–892.
61. Shin,S., Hyun,K., Kim,J. and Hohng,S. (2018) ATP binding to Rad5 initiates replication fork reversal by inducing the unwinding of the leading arm and the formation of the Holliday Junction. *Cell Rep.*, **23**, 1831–1839.
62. Shen,M., Dhingra,N., Wang,Q., Cheng,C., Zhu,S., Tian,X., Yu,J., Gong,X., Li,X., Zhang,H., *et al.* (2021) Structural basis for the multi-activity factor Rad5 in replication stress tolerance. *Nat. Commun.*, **12**, 321.
63. Kile,A.C., Chavez,D.A., Bacal,J., Eldirany,S., Korzhnev,D.M., Bezsonova,I., Eichman,B.F. and Cimprich,K.A. (2015) HLTF's ancient HIRAN domain binds 3′ DNA ends to drive replication fork reversal. *Mol. Cell*, **58**, 1090–1100.
64. Achar,Y.J., Balogh,D., Neculai,D., Juhasz,S., Morocz,M., Gali,H., Dhe-Paganon,S., Venclovas,Č. and Haracska,L. (2015) Human HLTF mediates postreplication repair by its HIRAN domain-dependent replication fork remodelling. *Nucleic Acids Res.*, **43**, 10277–10291.
65. Lopes,M., Cotta-Ramusino,C., Pellicioli,A., Liberi,G., Plevani,P., Muzi-Falconi,M., Newlon,C. and Foiani,M. (2001) The DNA replication checkpoint response stabilizes stalled replication forks. *Nature*, **412**, 557–561.
66. Tercero,J.A., Longhese,M.P. and Diffley,J.F. (2003) A central role for DNA replication forks in checkpoint activation and response. *Mol. Cell*, **11**, 1323–1336.
67. den Brave,F., Cairo,L.V., Jagadeesan,C., Ruger-Herreros,C., Mogk,A., Bukau,B. and Jentsch,S. (2020) Chaperone-mediated protein disaggregation triggers proteolytic clearance of intra-nuclear protein inclusions. *Cell Rep.*, **31**, 107680.
68. Claeys Bouuaert,C., Pu,S., Wang,J., Oger,C., Daccache,D., Xie,W., Patel,D.J. and Keeney,S. (2021) DNA-driven condensation assembles the meiotic DNA break machinery. *Nature*, **592**, 144–149.


**Received:** August 22, 2023. **Revised:** November 21, 2023. **Editorial Decision:** November 21, 2023. **Accepted:** November 23, 2023